NASA Contractor Report 165651

NASA-CR-165651
19810012492

Aerodynamic Prediction Techniques for Hypersonic Configuration Design

ROCKWELL INTERNATIONAL CORPORATION
Los Angeles, California 90009

CONTRACT NAS1-15820
MARCH 1981

National Aeronautics and
Space Administration

Langley Research Center
Hampton, Virginia 23665

NASA Contractor Report 165651

Aerodynamic Prediction Techniques for Hypersonic Configuration Design

ROCKWELL INTERNATIONAL CORPORATION
Los Angeles, California 90009

CONTRACT NAS1-15820
MARCH 1981

National Aeronautics and
Space Administration

Langley Research Center
Hampton, Virginia 23665

FOREWORD

This final report was prepared by the Aerodynamics Group of the North American Aircraft Division and the Fluid Mechanics Section of the Science Center of Rockwell International, Los Angeles, California for the Langley Research Center, National Aeronautics and Space Administration, Hampton Virginia. The work was performed under Contract No. NAS1-15820, "Extend and Develop Second Order and Full Potential Analyses as Aero Prediction Techniques for Hypersonic Configuration Design." Mr. Clyde L. W. Edwards and Mr. Gregory Riebe were the Project Monitors of this contract.

Mr. E. Bonner was the Program Manager; Drs. W. C. Clever, S. Chakravarthy, and V. Shankar served as Principal Investigators.

SUMMARY

An investigation of approximate theoretical techniques for predicting aerodynamic characteristics and surface pressures for relatively slender vehicles at moderate hypersonic speeds was performed. Emphasis was placed on approaches that would be responsive to preliminary configuration design level of effort. Potential theory was examined in detail to meet this objective.

Numerical pilot codes were developed for relatively simple three dimensional geometries to evaluate the capability of the approximate equations of motion considered. Results from the computations indicate good agreement with higher order solutions and experimental results for a variety of wing, body, and wing-body shapes for values of the hypersonic similarity parameter $M\delta$ approaching one.

TABLE OF CONTENTS

1. INTRODUCTION

An examination of the literature for airbreathing hypersonic concepts provides an indication of the flexibility and generality required for a prediction technique. Typical configuration development variables include wing section, incidence, height, dihedral, planform, effectiveness of longitudinal control surfaces for trim, effectiveness of empennage for directional stability, and propulsion system-airframe interactions.

State-of-the-art response to these prediction requirements is provided by hypersonic impact methods as well as linearized analysis and design algorithms. These approaches can treat significant geometry complexity with minimum response time and cost, with efficient predicted data coverage in terms of Mach number, angle of attack, trim deflection, yaw angle, etc. Shortcomings are present, however, in both the impact and linearized methods. For the former, interference between surface elements is totally ignored in implementations such as classical Newtonian, tangent wedge, and cone theories. Cross-flow interactions and stagnation point singularities are also implicitly disregarded. In the latter, shocks, vorticity, and entropy wakes and layers are excluded. Furthermore, superposition of elementary solutions such as those for thickness and angle of attack freely used in linear models are, strictly speaking, invalid at hypersonic speeds.

A need exists for new aerodynamic prediction techniques to use in the optimization of air vehicles designed to travel at hypersonic speeds. Propulsion, structure, and cooling considerations limit the range of cruise Mach numbers to be considered to between 4 and 8. One requirement of a new aerodynamic prediction technique is that it be more accurate than simple non-interfering panel methods. Another specification is that it be more computationally efficient than currently available explicit finite-difference methods so that it can be incorporated into a practical design procedure. The new approach should include enough of the physics of the flow to allow realistic optimization and should permit consideration of appropriate interactions between components of promising hypersonic arrangements, since this has been found to be the key to increasing aerodynamic efficiency at supersonic speeds. Less exact non-linear theoretical formulations hold the promise of meeting this objective and providing economic design codes which are responsive to preliminary vehicle definition efforts.

2. LIST OF SYMBOLS*

$\bar{c}$	mean aerodynamic chord
C_D	drag coefficient, $\frac{D}{qS}$
C_L	lift coefficient, $\frac{L}{qS}$
C_m	pitching moment coefficient, $\frac{M}{qS\bar{c}}$
C_P	pressure coefficient, $\frac{P-P_\infty}{q_\infty}$
D	drag
L	lift
M	Mach number or moment
P	static pressure
q	dynamic pressure
S	reference area
α	angle of attack
δ	flow deflection angle

SUBSCRIPTS

∞	free stream

*Additional specialized nomenclature is defined in the theoretical sections

3. METHODOLOGY

Emphasis is placed on approximate theoretical approaches which are capable of treating relatively general three dimensional problems but still sufficiently simple to be responsive to vehicle preliminary design efforts. The basic intent of the methodolgy is to produce future improvement in lift-drag ratio of hypersonic cruise vehicles. As a result of the strong impact that favorable interference has had on supersonic design and the use of such concepts in recent advanced hypersonic aircraft studies, candidate analysis should be general enough to systematically treat such problems. Finally, interest in high aerodynamic efficiency emphasizes relatively slender configurations at modest angle of attack; that is, moderate values of the hypersonic similarity parameter.

Theoretical effort was recently undertaken (1) to advance hypersonic aerodynamic prediction capability at the preliminary design level. A numerical three-dimensional second-order refinement of the Prandtl-Glauert model proposed by Van Dyke (2) was developed as a first step up from linear theory. Such a formulation incorporates nonlinear behavior but retains the isentropic approximimation. This approach is known to extend the prediction success for airfoil and cone surface pressure to substantially higher values of the hypersonic similarity parameter than first-order theory. Typical three dimensional prediction improvement provided by the numerical second-order analysis is presented in figures 1 and 2. These results indicate sufficient promise to pursue extension of the analysis to treat simple wing-body combinations. In addition, the study of second-order potential theory indicates that the next level of theoretical richness vis-a-vis a full potential equation of motion formulation should be explored as a means of removing edge singularities and improving treatment of characteristic surfaces.

Hypersonic small disturbance theory was considered in an earlier study (1) in recognition of the progressive non-isentropic behavior of the flow as the value of the hypersonic similarity parameter increases. Finite difference analysis of this approximation (3) indicated that the solution was essentially as complex as that for the Euler equation and thus would not be particularly responsive to preliminary design level of effort. This approach was not pursued in the present study on the basis of this finding and the previously cited success of potential analysis at moderate hypersonic conditions.

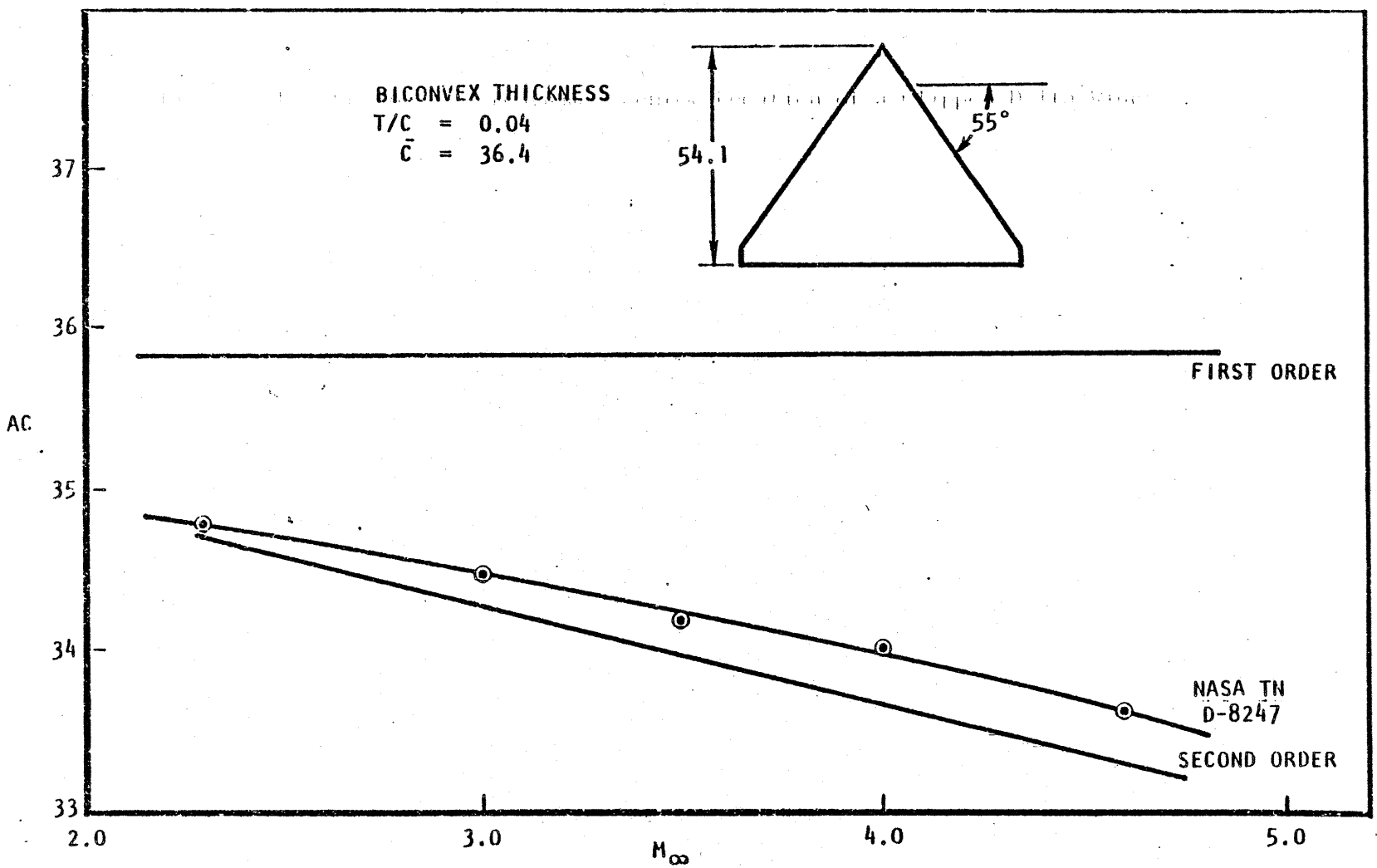

Figure 3.1. Predicted Aerodynamic Center Location of a Clipped Delta Wing

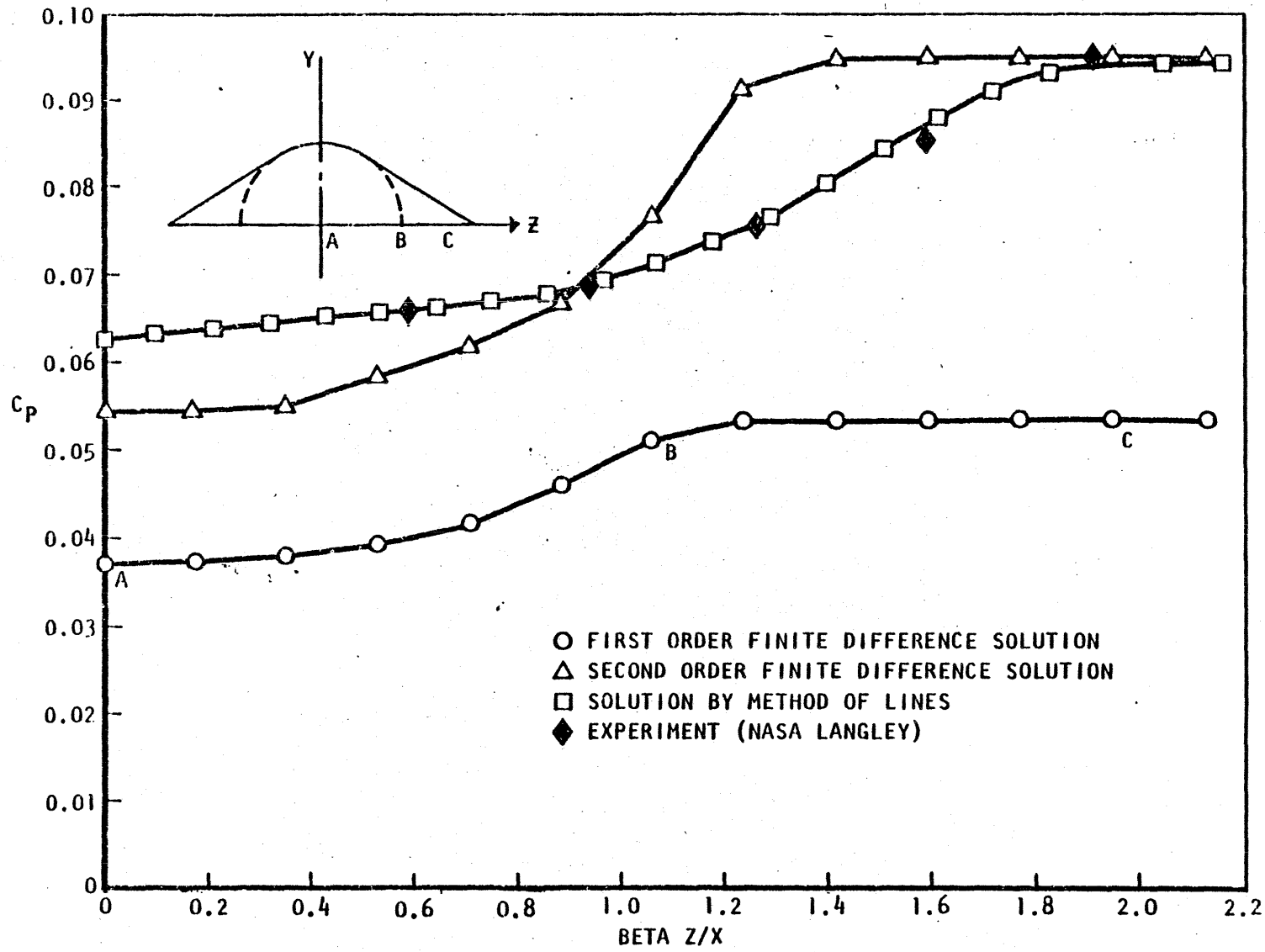

Figure 3.2. Predicted Compression Surface Pressure for a 70° Sweep Delta Wing at M = 6 and α = 8°

4. SECOND ORDER POTENTIAL ANALYSIS

4.1 APPROACH

The solution accurate to second order for the flow around wing-body combinations of aerodynamic interest may be represented by the velocity potential, Φ, written as the sum of the first and second order velocity potentials.

$$\Phi(x,y,z) = \phi(x,y,z) + \phi^{(2)}(x,y,z)$$

The condition of no flow through the boundary requires that

$$\left[\cos\alpha_\infty \vec{e}_x + \sin\alpha_\infty \vec{e}_z + \nabla\Phi\right] \cdot \vec{n} = 0$$

on the surface of the configuration. The solution, ϕ, accurate to first order, must satisfy the Prandtl-Glauert equation,

$$\Box^2\phi = \left\{(1-M_\infty^2)\frac{\partial^2}{\partial x^2} + \frac{\partial^2}{\partial y^2} + \frac{\partial^2}{\partial z^2}\right\}\phi = 0$$

and the the boundary condition

$$\left\{\vec{e}_x + \alpha_\infty \vec{e}_z + \nabla\phi\right\} \cdot \vec{n} = 0$$

on the surface. For the configurations of interest the aerodynamic surfaces are assumed to be thin, and the first order boundary condition is satisfied on the mean camber line in accordance with thin wing theory.

$$\frac{\partial\phi}{\partial n} = \frac{\partial\psi}{\partial x} - \alpha_\infty \cos\Lambda$$

Such a solution may be obtained by placing source and doublet singularities of appropriate strength on or inside the surface of the configuration.

The method used in this report to obtain first order solutions utilized axial singularities and quadrilateral source panels on the body surface in conjunction with quadrilateral source and vortex panels to represent the (thin) aerodynamic surfaces. The vortex panels, used to represent lift, were of constant strength, while the source panels, used to represent thickness,

could be made to vary linearly in either the chordwise or spanwise direction. The vortex panel and body source panel strengths where obtained by solving a set of simultaneous linear equations and thereby satisfying the boundary conditions at a set of control points. When the panel singularity strengths were obtained the flow properties could be obtained anywhere in the field. The second order potential, $\phi^{(2)}$, utilizes the first order solution. It must satisfy the nonhomogeneous Prandtl-Glauert equation

$$\Box^2 \phi^{(2)} = M_\infty^2 \frac{\partial}{\partial x} \left\{ \left[(1-M_\infty^2) + \frac{\gamma+1}{2} M_\infty^2 \right] \phi_x^2 + \phi_y^2 + \left[\phi_z + \alpha_\infty \right]^2 \right\}$$

as well as enable the boundary conditions to be satisfied to second order on the surface.

A second order solution using the source volume formulation described in reference 1, encounters numerical difficulties for complex configurations, wings with subsonic edges, and supersonic wing-body configurations. The primary reason is that source volume strengths require the calculation of spatial derivatives, and these cannot be obtained accurately enough from the first order solution when using the panel formulation. In addition the velocity discontinuities present in supersonic flow are accentuated, since the discontinuities introduced by the panel corners and edges do not attenuate with distance. Also no reasonable mesh density of spatial source volumes can properly account for the large gradients in flow properties near subsonic edges.

Therefore the second order solution was obtained using an approximate method which does not require the use of a spatial distribution of sources. This solution can be used even when large gradients are present (e.g. with subsonic edges). The solution is a three dimensional modification of the exact second order solution for the pressure coefficient on thin airfoils in two dimensions.

$$\frac{\theta-\theta_\infty}{\frac{1}{2}\rho_\infty U_\infty^2} = C_p(x,y) = -2 \left\{ \phi_x + \mathcal{R}(M) \left[\frac{1}{2}(1-M_\infty^2)\phi_x^2 + \frac{1}{2}\phi_y^2 + \frac{1}{2}\phi_z^2 + \psi \phi_{xz} + \phi_y \right] \right\}_{z=0}$$

where $\Box^2 \phi = 0$, $\qquad \mathcal{R}(M) = \frac{1}{(1-M^2)} \left[1 + \frac{\gamma+1}{4} \frac{M^4}{(1-M^2)} \right]$

and $$\phi_z(x,y,0) = (1-M_\infty^2)\phi_x \psi_x - \phi_y \psi_y + \psi \left[(1-M_\infty^2)\phi_{xx} + \phi_{yy} \right]$$

$\psi(x,y)$ represents the upper or lower surface of the airfoil. This solution, in effect, represents a local type solution, and all first order velocities represented above should be in a coordinate system rotated to make the z-axis normal to the local surface (e.g. with nonplanar configurations), but with no

local angle of incidence.

The derivation for this method of solution is presented in section 4.3, and the derivation for the exact two dimensional solution, from ref 2, is presented in section 4.2. The solution uses only the first order flow properties on the aerodynamic surfaces in conjunction with another first order type solution to the homogeneous Prandtl-Glauert equation. This other first order type solution is necessary to satisfy the boundary condition to second order.

$$\frac{\partial \phi}{\partial z} = \phi_z = \psi_x - \alpha_\infty$$

$$\frac{\partial \phi^{(2)}}{\partial z} = \phi_x \psi_x + \phi_y \psi_y + \psi \left[(1-M_\infty^2)\phi_{xx} + \phi_{yy} \right]$$

A particular solution using axial line sources, accurate to second order, was used to help represent the body.

$$\phi^{(2)}(x,r) = M_\infty^2 \phi_x \left[\phi - \frac{\gamma+1}{2} \frac{M_\infty^2}{1-M_\infty^2} r \phi_r \right] - \frac{1}{4} M_\infty^2 r \phi_r^3$$

This particular solution satisfies the second order axisymmetric nonhomogeneous Prandtl-Glauert equation to second order.

$$\Box^2 \phi^{(2)} = M_\infty^2 \frac{\partial}{\partial x} \left\{ \left[(1-M_\infty^2) + \frac{\gamma+1}{2} M_\infty^2 \right] \phi_x^2 + \phi_r^2 \right\} + M_\infty^2 \phi_{rr} \phi_r^2$$

where $\phi(x,r)$ is the first order solution to an equivalent axisymmetric body. This particular solution was combined with a solution to the homogeneous equation,

$$\Box^2 \hat{\phi}^{(2)} = \left\{ (1-M_\infty^2) \frac{\partial^2}{\partial x^2} + \frac{1}{r} \frac{\partial}{\partial r} + \frac{\partial^2}{\partial r^2} + \frac{1}{r^2} \frac{\partial^2}{\partial \theta^2} \right\} \hat{\phi}^{(2)} = 0$$

in order to satisfy the boundary conditions.

The second order accurate axisymmetric axial flow solution was combined with first order cross flow and axial solutions using the body paneling to

obtain the pressures on the body. The resulting solution is actually a hybrid solution combining second order accurate axial velocities with first order non-axisymmetric and cross flow velocities. Although a second order pressure coefficient is sufficient for plane type flows, for flows around bodies the exact isentropic pressure formula:

$$C_p = \frac{1}{\frac{1}{2}\gamma M_\infty^2}\left\{\left[1 - \frac{\gamma-1}{2}M_\infty^2\left(2u+u^2+v^2+w^2+2\alpha_\infty w\right)\right]^{\frac{\gamma}{\gamma-1}} - 1\right\}$$

was found to result in far more accurate pressure predictions when used to calculate flow about cones.

In a sense, the second order requirements on the body are not as stringent as on the aerodynamic surfaces since the boundary conditions on the body are satisfied on the actual surface, rather than the mean camber line, and the cross flow velocities may be small compared to the axial velocities. In addition the nonlinear expression for Cp in terms of the velocities is used on the body. The terms missing from the complete second order solution on the body are due to the second order non-axisymmetric perturbation velocities from the surfaces and from the non-homogeneous Prandtl-Glauert equation.

4.2 EXACT TWO DIMENSIONAL ANALYSIS

Consider flow past a thin airfoil at angle of attack $\alpha = \alpha_0 + \alpha_\infty$, where α_0 and α_∞ are the inclinations of the mean camber line and the free stream with respect to the x-axis.

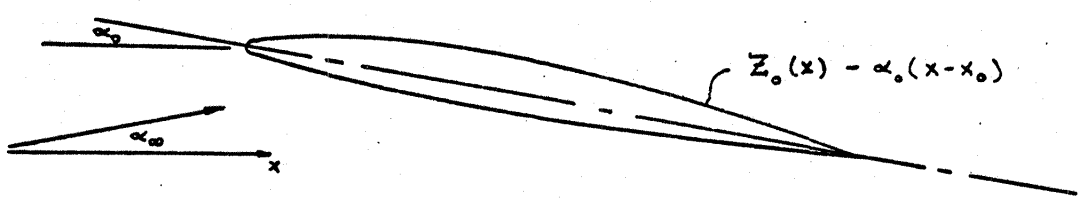

To second order the solution may be written

$$\Phi(x,z) = \phi(x,z) + \phi^{(2)}(x,z)$$

where ϕ and $\phi^{(2)}$ are solutions to

$$\Box^2\phi = \left\{(1-M_\infty^2)\frac{\partial^2}{\partial x^2} + \frac{\partial^2}{\partial z^2}\right\}\phi = 0$$

and

$$\Box^2 \phi^{(2)} = M_\infty^2 \frac{\partial}{\partial x} \left\{ \left[(1-M_\infty^2) + \frac{\gamma+1}{2} M_\infty^2 \right] \phi_x^2 + \left[\phi_z + \alpha_\infty \right]^2 \right\}$$

with boundary conditions

$$\phi_z(x,0) = Z_o'(x) - \alpha_o - \alpha_\infty$$

$$\phi_z^{(2)}(x,0) = \left[Z_o'(x) - \alpha_o \right] \phi_x(x,0) + (1-M_\infty^2) \left[Z_o(x) - \alpha_o (x - x_o) \right] \phi_{xx}(x,0)$$

To second order the pressure coefficient on the surface is

$$C_p = -2 \left\{ \phi_x(x,0) + \phi_x^{(2)}(x,0) + \frac{1}{2} \left[(1-M_\infty^2) \phi_x^2(x,0) + \left[\phi_z(x,0) + \alpha_\infty \right]^2 - \alpha_\infty^2 \right] + \left[Z_o(x) - \alpha_o (x - x_o) \right] \phi_{xz}(x,0) \right\}$$

To facilitate the solution we define

$$\Psi(x,z) = \int_{-\infty}^{x} \phi_z(\xi, z)\, d\xi \qquad \Psi_x = \phi_z \qquad \Psi_z = -(1-M_\infty^2)\, \phi_x$$

and

$$\Phi(x,z) \text{ such that} \qquad \Phi_x = \frac{1}{2} \left[(1-M_\infty^2) \phi_x^2 - \phi_z^2 \right] \qquad \Phi_z = (1-M_\infty^2) \phi_x \phi_z$$

Therefore $\Phi_{xz} = \Phi_{zx}$ and

$$\Box^2 \Psi = 0 \qquad \Box^2 \Phi = 0$$

Also

$$\Box^2(\phi_x\phi_z) = 0$$

$$\Box^2(\psi\phi_z) = (1-M_\infty^2)\left[(1-M_\infty^2)\phi_x^2 + \phi_z^2\right]_x \qquad [\ ]_x = \frac{\partial}{\partial x}[\ ]$$

$$\Box^2(z\phi_x\phi_z) = -\left[(1-M_\infty^2)\phi_x^2 - \phi_z^2\right]_x$$

$$\Box^2(x\phi_z) = (1-M_\infty^2)\,\Box^2(z\phi_x) = 2(1-M_\infty^2)\phi_{zx}$$

The boundary conditions can be rewritten

$$\phi_z(x,0) = \psi_x - \alpha_0 - \alpha_\infty$$

$$\phi_z^{(2)}(x,0) = \phi_x(\phi_z+\alpha_\infty) + (1-M_\infty^2)\phi_{xx}\left[\psi - \psi_0 + \alpha_\infty x\right]$$

and

$$C_p = -2\left\{\phi_x + \phi_x^{(2)} + \tfrac{1}{2}\left[(1-M_\infty^2)\phi_x^2 + (\phi_z+\alpha_\infty)^2 - \alpha_\infty^2\right] + \phi_{xz}\left[\psi - \psi_0 + \alpha_\infty x\right]\right\}$$

$\phi^{(2)}(x,z)$ may be written as the sum of a particular integral and a solution to the homogeneous equation.

$$\phi^{(2)}(x,z) = \phi_p^{(2)}(x,z) + \frac{1}{(1-M_\infty^2)}\left[1 + \frac{\gamma+1}{4}\frac{M_\infty^4}{(1-M_\infty^2)}\right]\phi_H^{(2)}(x,z)$$

The particular integral may be written immediately

$$\phi_p^{(2)}(x,z) = \frac{M_\infty^2}{(1-M_\infty^2)}\left[1 + \frac{\gamma+1}{4}\frac{M_\infty^2}{(1-M_\infty^2)}\right]\left[(\psi - \psi_0 + \alpha_\infty x)\phi_z + \phi\right]$$

$$- \frac{\gamma+1}{4}\frac{M_\infty^4}{(1-M_\infty^2)}\left[z\phi_x(\phi_z+\alpha_\infty)\right]$$

because

$$\Box^2\phi_p^{(2)} = M_\infty^2\left[1 + \frac{\gamma+1}{4}\frac{M_\infty^2}{(1-M_\infty^2)}\right]\left[(1-M_\infty^2)\phi_x^2 + (\phi_z+\alpha_\infty)^2\right]_x$$

$$+ \frac{\gamma+1}{4}\frac{M_\infty^4}{(1-M_\infty^2)}\left[(1-M_\infty^2)\phi_x^2 - (\phi_z+\alpha_\infty)^2\right]_x$$

$$= M_\infty^2\frac{\partial}{\partial x}\left\{\left[(1-M_\infty^2) + \frac{\gamma+1}{2}M_\infty^2\right]\phi_x^2 + (\phi_z+\alpha_\infty)^2\right\}$$

and at $z = 0$

$$\phi^{(2)}_{P_x} = \frac{M_\infty^2}{(1-M_\infty^2)}\left[1+\frac{\gamma+1}{4}\frac{M_\infty^2}{1-M_\infty^2}\right]\left\{\frac{1}{2}\left[(1-M_\infty^2)\phi_x^2+(\phi_z+\alpha_\infty)^2-\alpha_\infty^2\right]+\phi_{zx}\left[\psi-\psi_0+\alpha_\infty x\right]\right\}$$

$$\phi^{(2)}_{P_z} = \phi_x(\phi_z+\alpha_\infty)+(1-M_\infty^2)\left[\psi-\psi_0+\alpha_\infty x\right]\phi_{xx} - \left[1+\frac{\gamma+1}{4}\frac{M_\infty^4}{1-M_\infty^2}\right]\left[\phi_x(\phi_z+\alpha_\infty)+(\psi-\psi_0+\alpha_\infty x)\phi_{xx}\right]$$

therefore the solution for $\phi^{(2)}$ is complete if

$$\Box^2 \phi^{(2)}_H = 0$$

and at $z = 0$

$$\phi^{(2)}_{H_z} = \left[\phi_x(\phi_z+\alpha_\infty)+(\psi-\psi_0+\alpha_\infty x)\phi_{xx}\right](1-M_\infty^2)$$

therefore

$$C_p = -2\left\{\phi_x+\frac{1}{(1-M_\infty^2)}\left[1+\frac{\gamma+1}{4}\frac{M_\infty^4}{(1-M_\infty^2)}\right]\left[\frac{1}{2}(1-M_\infty^2)\phi_x^2+\frac{1}{2}(\phi_z+\alpha_\infty)^2-\frac{1}{2}\alpha_\infty^2 + \phi_{xz}(\psi-\psi_0+\alpha_\infty x)+\phi^{(2)}_{H_x}\right]\right\}$$

The angle of incidence of the free stream may be eliminated from the above expression. This means the solution to order two will depend only on $\alpha = \alpha_0 + \alpha_\infty$.

Let

$$(1-M_\infty^2)\phi^{(2)}_H = (1-M_\infty^2)\phi^{(2)}_0 + \left[(1-M_\infty^2)z\phi_x - x\phi_z\right]\alpha_\infty$$

then since

$$\Box^2\left[(1-M_\infty^2)z\phi_x - x\phi_z\right] = 0$$

$$\Box^2 \phi^{(2)}_0 = 0$$

and at $z = \emptyset$

$$\phi^{(2)}_{o_z} = \phi_x \phi_z + (\psi - \psi_o)\phi_{xx}$$

$$(1-M_\infty^2)\phi^{(2)}_{H_x} = (1-M_\infty^2)\phi^{(2)}_{o_x} - \alpha_\infty [x\phi_{zx} + \phi_z]$$

and therefore

$$C_p = -2\left\{ \phi_x + \frac{1}{(1-M_\infty^2)}\left[1 + \frac{\gamma+1}{4}\frac{M_\infty^4}{(1-M_\infty^2)}\right]\left[\tfrac{1}{2}(1-M_\infty^2)\phi_x^2 + \tfrac{1}{2}\phi_z^2 + \phi_{xz}(\psi-\psi_o) + \phi^{(2)}_{o_x}\right]\right\}$$

Since each term in the above expression depends only upon $\alpha = \alpha_o + \alpha_\infty$, the pressure coefficient to second order is the same whether the free stream or the airfoil is placed at an angle of incidence. Replacing ψ with its expression in terms of geometry yields the expression,

$$C_p = -2\left\{ \phi_x + \frac{1}{(1-M_\infty^2)}\left[1 + \frac{\gamma+1}{4}\frac{M_\infty^4}{(1-M_\infty^2)}\right]\left[\tfrac{1}{2}(1-M_\infty^2)\phi_x^2 + \tfrac{1}{2}\phi_z^2 + \phi_{zx}(Z_o(x) - \alpha x) + \phi^{(2)}_{o_x}\right]\right\}$$

$$\phi^{(2)}_{o_z}(x,o) = (1-M_\infty^2)\phi_x\phi_z + (1-M_\infty^2)[Z_o(x) - \alpha x]\phi_{xx}$$

4.3 EXACT SKEWED WING ANALYSIS

Let $\hat{\phi}(\xi, \zeta)$ be the first order solution which satisfies

$$\Box^2\hat{\phi} = \left\{(1-M^2)\frac{\partial^2}{\partial\xi^2} + \frac{\partial^2}{\partial\zeta^2}\right\}\hat{\phi} = 0$$

$$\hat{\phi}_\zeta(\xi, o) = Z_{1_\xi}(\xi) - \hat{\alpha}_o - \hat{\alpha}_\infty$$

then Cp to second order may be written:

$$\hat{C}_p = -2\left\{ \hat{\phi}_\zeta + \mathcal{R}(M)\left[\tfrac{1}{2}(1-M^2)\hat{\phi}_\xi^2 + \tfrac{1}{2}(\hat{\phi}_\zeta + \alpha_\infty)^2 - \tfrac{1}{2}\hat{\alpha}_\infty^2 + [Z - \hat{\alpha}_o(\xi - \xi_o)]\hat{\phi}_{\xi\zeta} + \phi_\xi\right]\right\}_{\zeta=o}$$

where $\hat{\phi}(\xi,\zeta)$ is a solution to

$$\Box^2 \hat{\phi} = 0 \qquad \hat{\phi}_\zeta(\xi,0) = (1-M^2)\left\{\hat{\phi}_\xi[\hat{\phi}_\zeta + \hat{\alpha}_\infty] + [\xi - \hat{\alpha}_0(\xi-\xi_0)]\hat{\phi}_{\xi\xi}\right\}$$

and

$$\mathcal{K}(M) = \frac{1}{(1-M^2)}\left[1 + \frac{\gamma+1}{4}\frac{M^4}{(1-M^2)}\right]$$

This exact two dimensional solution may be applied to an infinite skewed wing in three dimensions because with a rotation of coordinates all flow properties depend only on two dimensions. Consider the following transformation.

$$\xi = \frac{1}{\sqrt{1+T^2}}(x - Ty) \qquad \frac{\partial}{\partial \xi} = \frac{1}{\sqrt{1+T^2}}\left(\frac{\partial}{\partial x} - T\frac{\partial}{\partial y}\right)$$

$$\eta = \frac{1}{\sqrt{1+T^2}}(Tx + y) \qquad \frac{\partial}{\partial \eta} = \frac{1}{\sqrt{1+T^2}}\left(T\frac{\partial}{\partial x} + \frac{\partial}{\partial y}\right)$$

$$\zeta = z \qquad \frac{\partial}{\partial \zeta} = \frac{\partial}{\partial z}$$

$$x = \frac{1}{\sqrt{1+T^2}}(\xi + T\eta) \qquad \frac{\partial}{\partial x} = \frac{1}{\sqrt{1+T^2}}\left(\frac{\partial}{\partial \xi} + T\frac{\partial}{\partial \eta}\right)$$

$$y = \frac{1}{\sqrt{1+T^2}}(-T\xi + \eta) \qquad \frac{\partial}{\partial y} = \frac{1}{\sqrt{1+T^2}}\left(-T\frac{\partial}{\partial \xi} + T\frac{\partial}{\partial \eta}\right)$$

$$z = \zeta \qquad \frac{\partial}{\partial z} = \frac{\partial}{\partial \zeta}$$

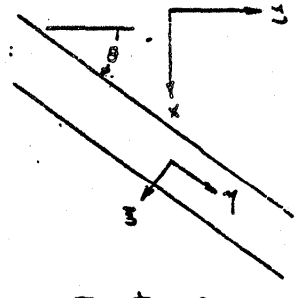

$T = \tan\theta$

$$\alpha = \frac{\hat{\alpha}}{\sqrt{1+T^2}} \qquad \phi(x,y,z) = \frac{\hat{\phi}(\xi,\zeta)}{\sqrt{1+T^2}} \qquad C_p(x,y) = \frac{\hat{C}_p(\xi)}{(1+T^2)}$$

$$M_\infty^2 = M^2(1+T^2) \qquad U_\infty^2 = U^2(1+T^2)$$

and since $\frac{\partial}{\partial \eta} = 0$, $\left[T\frac{\partial}{\partial x} + \frac{\partial}{\partial y}\right] = 0$

The two dimensional solution may be written in three dimensions as follows:

$$\frac{p-p_\infty}{\frac{1}{2}\rho_\infty U_\infty^2} = C_p(x,y) = -2\left\{ \phi_x + \mathcal{R}(M)\left[\tfrac{1}{2}(1-M_\infty^2)\phi_x^2 + \tfrac{1}{2}\phi_y^2 + \tfrac{1}{2}(\phi_z+\alpha_\infty)^2 - \tfrac{1}{2}\alpha_\infty^2 + [Z-\alpha_0(x-x_0)]\phi_{xz} + \Phi_x\right]\right\}$$

where

$$\phi_z(x,y,0) = Z_x(x,y) - \alpha_0 - \alpha_\infty$$

$$\Box^2\phi = \left[(1-M_\infty^2)\frac{\partial^2}{\partial x^2} + \frac{\partial^2}{\partial y^2} + \frac{\partial^2}{\partial z^2}\right]\phi(x,y,z) = 0$$

and

$$\Box^2\Phi = 0$$

$$\Phi_z(x,y,0) = (1-M_\infty^2)\phi_x[Z_x-\alpha_0] + \phi_y Z_y + [Z-\alpha_0(x-x_0)][(1-M_\infty^2)\phi_{xx} + \phi_{yy}]$$

However, the exact solution in three dimensions is:

$$C_p(x,y) = -2\left\{ \phi_x + \tfrac{1}{2}(1-M_\infty^2)\phi_x^2 + \tfrac{1}{2}\phi_y^2 + \tfrac{1}{2}(\phi_z+\alpha_\infty)^2 - \tfrac{1}{2}\alpha_\infty^2 + [Z-\alpha_0(x-x_0)]\phi_{xz} + \Phi_x + \Phi_x\right\}$$

$$\Phi_z(x,y,0) = \phi_x[Z_x-\alpha_0] + \phi_y Z_y + [Z-\alpha_0(x-x_0)][(1-M_\infty^2)\phi_{xx} + \phi_{yy}] + \Phi_z$$

$$\Box^2\Phi = 0$$

The only difference between the two solutions is Φ_x, with

$$\mathcal{R}(M) = \frac{1}{(1-M^2)}\left[1 + \frac{\gamma+1}{4}\frac{M^4}{(1-M^2)}\right]$$

multiplying the second order Cp terms, and the boundary conditions for $\bar{\Phi}$. The coefficient $(1-M_\infty^2)$ multiplying the $\phi_x\phi_z$ term is the factor which would be present if mass-flux boundary conditions were used, and the second term is due to the perturbations of the spatial source distribution,

$$\Box^2\bar{\Phi} = \rho(x,y,z) = M_\infty^2 \frac{\partial}{\partial x}\left\{\left[(1-M_\infty^2)+\frac{\gamma+1}{2}M_\infty^2\right]\phi_x^2 + \phi_y^2 + \phi_z^2\right\}$$

on the plane $z = \emptyset$.

When applied in three dimensions the transformed two dimensional equation should give the exact second order pressures whenever the flow is locally two dimensional and may be approximated by an infinite skewed system. The Mach number, M, used in calculating the coefficient $\mathcal{K}$ is equal to $M_\infty\cos\Theta$ (i.e. the normal Mach number). Whenever $M_\infty\cos\Theta$ is equal to unity, $\mathcal{K}$ becomes infinite, indicating the second order solution is not valid near $M = 1$. If M_∞ is used for calculating $\mathcal{K}$ the solution remains finite except near $M_\infty = 1$. Since $\mathcal{K}$ is a slowly varying function of M (see figure 4.1.1), except near $M = 1$, $\mathcal{K}(M_\infty)$ could be substituted for $\mathcal{K}(M_N)$ without much change in the result.

4.4 SOLUTION STRUCTURE

Consider a span station where second order characteristics are to be computed, and write all variables in a coordinate system rotated to make the z-axis normal to the local surface.

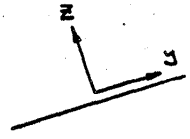

Since the first order solution is linear, the first order perturbation velocities can be considered to be the composed of four parts.

1. Contributions from all panels due to an incremental change in angle of attack (add load velocities).
2. The incremental contribution from all panels due to the twist and camber of the aerodynamic surfaces.
3. The velocity perturbations due to thickness.
4. The velocity perturbations due to the body in axial flow.

Some components have an odd or even part with respect to the local z = 0 plane. Therefore we can write,

$$\phi_x = u = \alpha[u_\alpha \pm \Delta u_\alpha] + \gamma[u_\gamma \pm \Delta u_\gamma] + \tau[u_\tau \pm \Delta u_\tau] + [u_b \pm \Delta u_b]$$

$$\phi_y = v = \alpha[v_\alpha \pm \Delta v_\alpha] + \gamma[v_\gamma \pm \Delta v_\gamma] + \tau[v_\tau \pm \Delta v_\tau] + [v_b \pm \Delta v_b]$$

$$\phi_z = w = \alpha w_\alpha + \gamma w_\gamma + \tau[w_\tau \pm \Delta w_\tau] + w_b$$

where $\pm$ indicate upper or lower surface. The contributions having a $\pm$ have an odd symmetry with respect to the local z = 0 plane.

The surface displacements ψ are composed of three parts.

1. Displacements due to angle of attack.
2. Displacements due to twist and camber.
3. Displacements due to thickness.

Therefore we can write,

$$\psi = \alpha\psi_\alpha + \gamma\psi_\gamma \pm \tau\psi_\tau$$

All contributions to the second order terms are composed of products of first order terms. These terms will have either an odd or an even symmetry with respect to the local z = 0 plane. The odd symmetry terms in th Cp expression contribute to a ΔCp across the aerodynamic surface while the even symmetry terms contribute to an equal Cp on each side.

$$Cp = -2\phi_x + Cp^{(2)}$$

$$Cp^{(2)} = -2\mathcal{R}(M)\left[\tfrac{1}{2}(1-M_\infty^2)\phi_x^2 + \tfrac{1}{2}\phi_y^2 + \tfrac{1}{2}(\phi_z+\alpha_\infty)^2 - \tfrac{1}{2}\alpha_\infty^2 + [\psi - \alpha_0(x-x_0)]\phi_{zx} + \phi_x\right]$$

and

$$\phi_x^2 = \alpha^2[u_\alpha^2 + (\Delta u_\alpha)^2] + \gamma^2[u_\gamma^2 + (\Delta u_\gamma)^2] + \tau^2[u_\tau^2 + (\Delta u_\tau)^2] + [u_b^2 + (\Delta u_b)^2]$$
$$+2\alpha\gamma[u_\alpha u_\gamma + \Delta u_\alpha \Delta u_\gamma] + 2\alpha\tau[u_\alpha u_\tau + \Delta u_\alpha \Delta u_\tau] + 2\gamma\tau[u_\gamma u_\tau + \Delta u_\gamma \Delta u_\tau]$$
$$+2u_b[\alpha u_\alpha + \gamma u_\gamma + \tau u_\tau] + 2\Delta u_b[\alpha\Delta u_\alpha + \gamma\Delta u_\gamma + \tau\Delta u_\tau]$$
$$\pm 2\Big\{\alpha^2 u_\alpha \Delta u_\alpha + \gamma^2 u_\gamma \Delta u_\gamma + \tau^2 u_\tau \Delta u_\tau + u_b \Delta u_b$$
$$+\alpha\gamma[u_\alpha \Delta u_\gamma + u_\gamma \Delta u_\alpha] + \alpha\tau[u_\alpha \Delta u_\tau + u_\tau \Delta u_\alpha] + \gamma\tau[u_\gamma \Delta u_\tau + u_\tau \Delta u_\gamma]$$
$$+u_b[\alpha\Delta u_\alpha + \gamma\Delta u_\gamma + \tau\Delta u_\tau] + \Delta u_b[\alpha u_\alpha + \gamma u_\gamma + \tau u_\tau]\Big\}$$

$$\phi_z^2 = \alpha^2 \omega_\alpha^2 + \gamma^2 \omega_\gamma^2 + \tau^2 [\omega_\tau^2 + (\Delta\omega_\tau)^2] + \omega_b^2$$
$$+ 2\alpha\gamma\omega_\alpha\omega_\gamma + 2\alpha\tau\omega_\alpha\omega_\tau + 2\gamma\tau\omega_\gamma\omega_\tau$$
$$+ 2\omega_b[\alpha\omega_\alpha + \gamma\omega_\gamma + \tau\omega_\tau]$$
$$\pm 2\tau\Delta\omega_\tau[\alpha\omega_\alpha + \gamma\omega_\gamma + \omega_b]$$

$$\psi\phi_{xz} = \psi\psi_{xx} = \alpha^2\psi_\alpha\psi_{\alpha_{xx}} + \gamma^2\psi_\gamma\psi_{\gamma_{xx}} + \tau^2\psi_\tau\psi_{\tau_{xx}} + \alpha\gamma[\psi_\alpha\psi_{\gamma_{xx}} + \psi_\gamma\psi_{\alpha_{xx}}]$$
$$\pm \alpha\tau[\psi_\alpha\psi_{\tau_{xx}} + \psi_\tau\psi_{\alpha_{xx}}] \pm [\psi_\gamma\psi_{\tau_{xx}} + \psi_\tau\psi_{\gamma_{xx}}]$$

with similar terms for ϕ_y^2.

The expression ϕ_x is calculated from the second order boundary condition for ϕ. The odd symmetry second order boundary conditions will be satisfied by a homogeneous solution using source panels, while the even symmetry second order boundary conditions will be satisfied using vortex panels and will contribute to a net ΔCp across the surface.

$$\phi_z(x,y,0) = (1-M_\infty^2)\phi_x[\psi_x - \alpha_0] + \phi_y\psi_y + [\psi - \alpha_0(x-x_0)][(1-M_\infty^2)\phi_{xx} + \phi_{yy}]$$

where

$$\phi_{\sigma_z} = \frac{1}{2}[\phi_z^+ - \phi_z^-]$$

$$\phi_{\Gamma_z} = \frac{1}{2}[\phi_z^+ + \phi_z^-]$$

By setting the various coefficients α, γ, or τ equal to zero, the second order effect of various combinations of angle of attack, camber and thickness may be analyzed from the basic solutions. The terms Δu_τ and ω_τ are due to the lift due to thickness and are generally small, and in fact are zero for planar configurations. The terms Δu_b and w_b are the lift induced by the body in axial flow and are also in general small. For planar configurations or when there is symmetry about the $z = 0$ plane, the velocity expressions

simplify,

$$\phi_x = u = \alpha[u_\alpha \pm \Delta u_\alpha] + \gamma[v_\gamma \pm \Delta v_\gamma] + \tau u_\tau + u_b$$

$$\phi_y = v = \alpha[v_\alpha \pm \Delta v_\alpha] + \gamma[v_\gamma \pm \Delta v_\gamma] + \tau v_\tau + v_b$$

$$\phi_z = w = \alpha w_\alpha + \gamma w_\gamma \pm \tau \Delta w_\tau$$

and

$$\phi_x^2 = \alpha^2[u_\alpha^2 + (\Delta u_\alpha)^2] + \gamma^2[u_\gamma^2 + (\Delta u_\gamma)^2] + \tau^2 u_\tau^2 + u_b^2$$
$$+2\alpha\gamma[u_\alpha u_\gamma + \Delta u_\alpha \Delta u_\gamma] + 2\alpha\tau u_\alpha u_\tau + 2\gamma\tau u_\gamma u_\tau + 2u_b[\alpha u_\alpha + \gamma u_\gamma + \tau u_\tau]$$
$$\pm 2\left\{\alpha^2 u_\alpha \Delta u_\alpha + \gamma^2 u_\gamma \Delta u_\gamma + [\tau u_\tau + u_b][\alpha \Delta u_\alpha + \gamma \Delta u_\gamma]\right\}$$

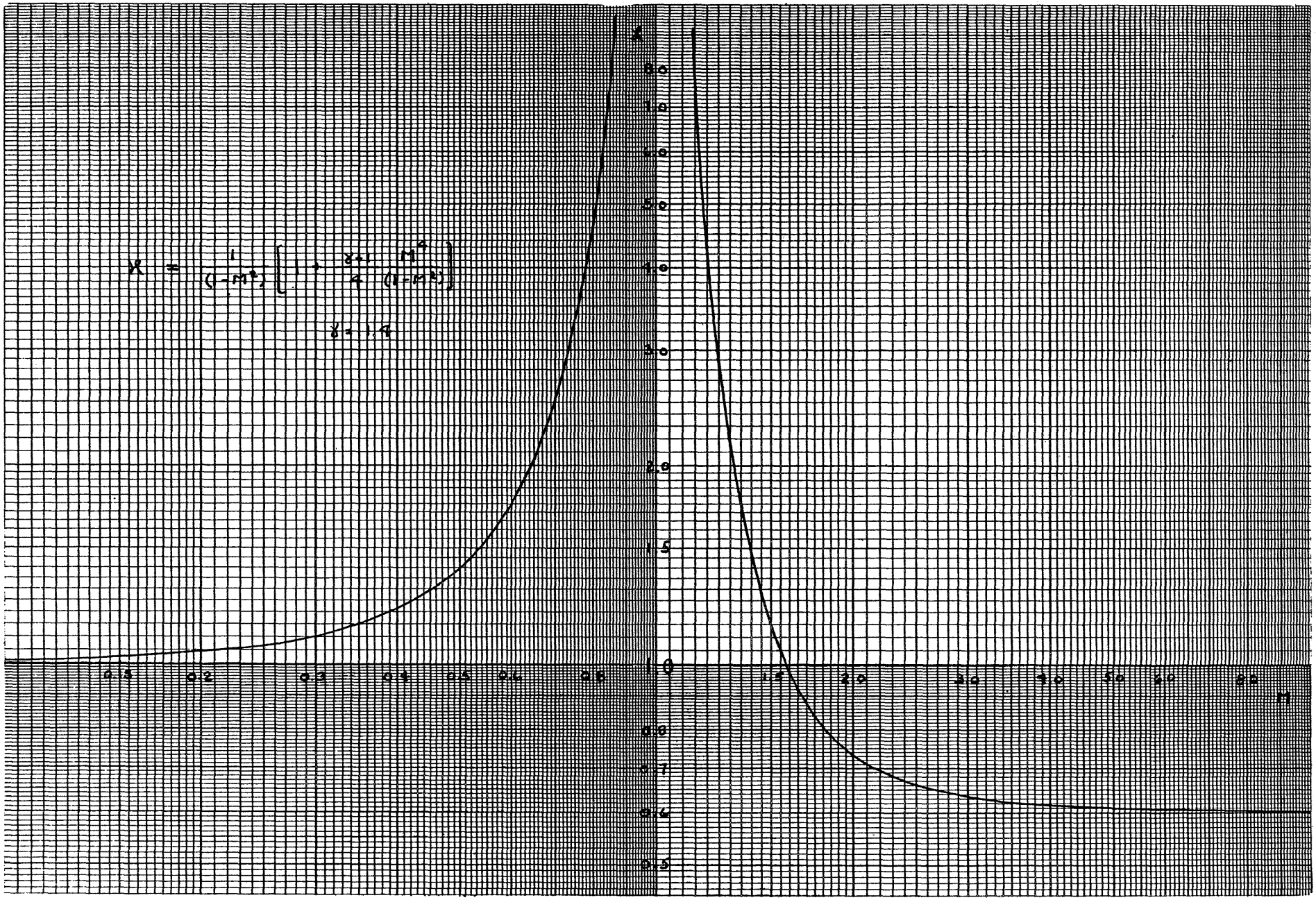

Figure 4.1.1. Second Order Coefficient χ

5. FULL POTENTIAL ANALYSIS

The full potential equation either in conservative form or nonconservative form is frequently used for the treatment of transonic flow fields, where the local Mach number in general does not exceed ~1.4. However, if the assumptions of irrotationality and isentropicity are reasonably valid then the full potential equation is expected to yield results comparable to Euler equations, even for supersonic/hypersonic flow fields.

The full potential equation can be obtained from the continuity of mass relation by assuming the flow to be irrotational and isentropic. In the Cartesian system (x,y,z), the continuity of mass can be written as

$$\frac{\partial(\rho u)}{\partial x} + \frac{\partial(\rho v)}{\partial y} + \frac{\partial(\rho w)}{\partial z} = 0 \qquad (5.1)$$

where ρu, ρv, and ρw represent mass flux in the x, y, and z directions, respectively. For an irrotational and isentropic flow, the density ρ, and the velocity components u, v, and w are expressed in terms of the velocity potential ϕ as

$$\left.\begin{aligned} u &= \phi_x \quad ; \quad v = \phi_y \quad ; \quad w = \phi_z \\ \rho &= \left[1 - \frac{\gamma-1}{2} M_\infty^2(\phi_x^2 + \phi_y^2 + \phi_z^2 - 1)\right]^{1/\gamma-1} \end{aligned}\right\} . \tag{5.2}$$

Here, the density and the velocity components are normalized with respect to the freestream values.

Equation (5.1) is said to be in conservation form. The nonconservative form of Eq. (5.1) can be obtained in the following manner. Differentiating the mass flux terms in Eq. (5.1), we get

$$\rho(u_x + v_y + w_z) + u\rho_x + v\rho_y + w\rho_z = 0 \tag{5.3}$$

where

$$\rho_x = - \frac{\rho}{a^2} (uu_x + vv_x + ww_x)$$

$$\rho_y = - \frac{\rho}{a^2} (uu_y + vv_y + ww_y)$$

$$\rho_z = - \frac{\rho}{a^2} (uu_z + vv_z + ww_z)$$

and a is the local speed of sound expressed as

$$a^2 = \frac{\rho^{\gamma-1}}{M_\infty^2} . \tag{5.4}$$

Substituting for ρ_x, ρ_y and ρ_z and writing u, v and w in terms of ϕ in Eq. (5.3), the nonconservative form of Eq. (5.1) can be written as

$$(a^2 - \phi_x^2)\phi_{xx} + (a^2 - \phi_y^2)\phi_{yy} + (a^2 - \phi_z^2)\phi_{zz}$$

$$- 2\phi_x\phi_y\phi_{xy} - 2\phi_x\phi_z\phi_{xz} - 2\phi_y\phi_z\phi_{yz} = 0 \quad . \quad (5.5)$$

The full potential equation can either be solved in conservation form (Eq. (5.1)) or nonconservative form (Eq. (5.5)). In general, conservation form is preferred because it allows for the correct weak solution (presence of discontinuities like shocks and slip surface) to form in the course of the calculation.

In this report, two different approaches will be described to solve the conservative full potential equation.

5.1 VECTOR APPROACH

Equation (5.1) contains three unknown variables: u, v and w. The density ρ is expressed in terms of the velocity as shown in Eq. (5.2). In the vector approach, the velocities u, v and w will be obtained by solving the following three equations:

$$(\rho u)_x + (\rho v)_y + (\rho w)_z = 0 \quad (5.6)$$

$$v_x - u_y = 0 \tag{5.7}$$

$$w_x - u_z = 0 \ . \tag{5.8}$$

Equation (5.6) is the same as Eq. (5.1) and Eqs. (5.7) and (5.8) are the irrotationality conditions. These three equations can be conveniently represented in a vector form as

$$E_x + F_y + G_z = 0 \tag{5.9}$$

where

$$E = \begin{bmatrix} \rho u \\ v \\ w \end{bmatrix} \quad , \quad F = \begin{bmatrix} \rho v \\ -u \\ 0 \end{bmatrix} \quad , \quad G = \begin{bmatrix} \rho w \\ 0 \\ -u \end{bmatrix}$$

Equation (5.9) is hyperbolic with respect to the direction x if the velocity component u is greater than the speed of sound. Assuming $u > a$, solution to Eq. (5.9) can be obtained by marching in the x direction using any stable and consistent finite-difference scheme. Equation (5.9) is in Cartesian frame. In order to apply the surface tangency condition at the actual body location, a body fitted coordinate transformation is essential. If we denote the coordinate transformation as

$$\sigma = \sigma(x) \quad ; \quad \eta = \eta(x,y,z) \quad ; \quad \xi = \xi(x,y,z) \tag{5.10}$$

then, the transformed equation corresponding to (5.9) can be written in conservation form as

$$\hat{E}_\sigma + \hat{F}_\xi + \hat{G}_\eta = 0 \tag{5.11}$$

where

$$\left.\begin{aligned} \hat{E} &= \frac{E}{J} \\ \hat{F} &= \frac{E\xi_x + F\xi_y + G\xi_z}{J} \\ \hat{G} &= \frac{E\eta_x + F\eta_y + G\eta_z}{J} \end{aligned}\right\} \tag{5.12}$$

and J is the Jacobian of the transformation

$$J = \xi_y\eta_z - \xi_z\eta_y \ . \tag{5.13}$$

In this report, Eq. (5.11) is solved using the MacCormack[4] predictor-corrector method assuming σ to be the time-like

hyperbolic direction. At every marching step, the E vector is advanced. Before calculating the F and G vector, the density ρ and the velocity components u, v and w must be extracted from the E vector. This decoding process is given here.

5.1.1 Decoding Procedure

$$E = \hat{E}J = \begin{pmatrix} e_1 = \rho u \\ e_2 = v \\ e_3 = w \end{pmatrix} \tag{5.14}$$

The velocities v and w are nothing but e_2 and e_3, respectively. The component u is obtained from the relation

$$u^{i+1} = u^i - \left[f(u) \Big/ \left(\frac{df}{du} \right) \right]^i \tag{5.15}$$

where i denotes the Newton iteration and f(u) is represented as

$$f(u) = Au^{\gamma+1} + Bu^{\gamma-1} + C = 0$$

where

$$A = \frac{\gamma-1}{2} M_\infty^2$$

$$B = \frac{\gamma-1}{2} M_\infty^2 (v^2 + w^2 - 1) - 1$$

$$C = (e_1)^{\gamma-1} .$$

Once u is computed from Eq. (5.15) the density is given by

$$\rho = \frac{e_1}{u} . \tag{5.16}$$

Usually, two or three iterations are enough for the recursions to converge in Eq. (5.15).

5.1.2 Shock Jump Relations for Potential Flow

In the present approach the outer shocks are treated as computational boundaries and fitted as part of the solution by satisfying the appropriate shock jump relations across them.

Let the shock be defined as a constant η surface.

$$\eta(x,y,z) = C . \tag{5.17}$$

The unit vector normal to the shock is then defined by (see Fig. 5.1)

$$N = (\eta_x \hat{i} + \eta_y \hat{j} + \eta_z \hat{k}) / \sqrt{\eta_x^2 + \eta_y^2 + \eta_z^2} \tag{5.18}$$

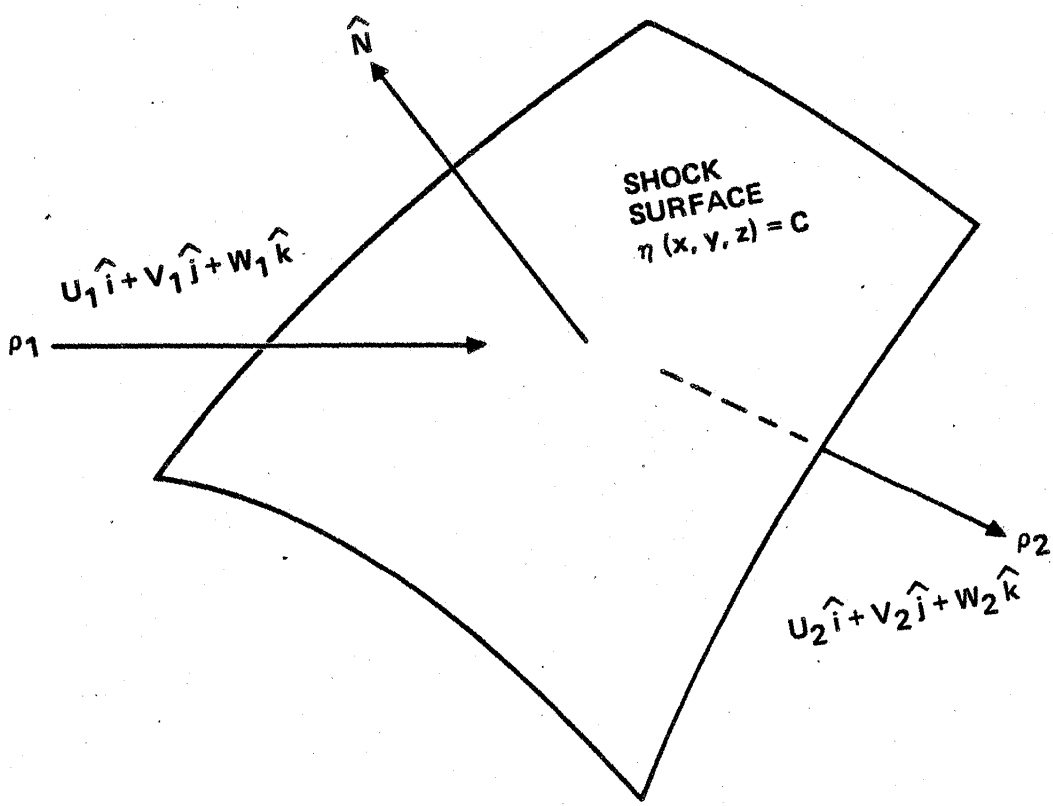

Figure 5.1. Shock Nomenclature

where $\hat{i}$, $\hat{j}$ and $\hat{k}$ are the Cartesian unit vectors. Let the dependent variables u_1, v_1, w_1, ρ_1 be known on the upstream side of the shock. For the discussion in this report, these are freestream values. Then, if the shock geometry defined by η_x, η_y and η_z is known, one should be able to compute ρ_2, u_2, v_2 and w_2 on the downstream side of the shock. On the other hand, if the density behind the shock, ρ_2, is known along with two of the direction cosines of the shock normal, say η_y and η_z, then η_x, u_2, v_2 and w_2 may be computed. These two situations may be termed the direct and inverse shock jump problems.

5.1.2.1 Direct Shock Jump Relations

η_x, η_y, η_z, u_1, v_1, w_1, $\rho_1 = 1.0$ are known.

$$a_1 = \rho_1^{\gamma-1}/M_\infty^2$$

$$U_{1N} = (u_1\hat{i} + v_1\hat{j} + w_1\hat{k}) \cdot \frac{(\eta_x\hat{i} + \eta_y\hat{j} + \eta_z\hat{k})}{\sqrt{\eta_x^2 + \eta_y^2 + \eta_z^2}}$$

$$M_s = |U_{1N}|/a_1$$

ρ_2 is computed by Newton iteration to satisfy

$$(\rho_2)^{\gamma+1} - \left(\frac{\gamma-1}{2} M_s^2 + 1\right)\rho_2^2 + \frac{\gamma-1}{2} M_s^2 = 0$$

$$u_2 = u_1 + U_{1N}\left(\frac{1}{\rho_2} - 1\right) \frac{\eta_x}{\sqrt{\eta_x^2 + \eta_y^2 + \eta_z^2}}$$

$$v_2 = v_1 + U_{1N}\left(\frac{1}{\rho_2} - 1\right) \frac{\eta_y}{\sqrt{\eta_x^2 + \eta_y^2 + \eta_z^2}} \qquad (5.19)$$

$$w_2 = w_1 + U_{1N}\left(\frac{1}{\rho_2} - 1\right) \frac{\eta_z}{\sqrt{\eta_x^2 + \eta_y^2 + \eta_z^2}}$$

5.1.2.2 Inverse Shock Jump Relations

Two out of η_x, η_y, η_z are known along with ρ_2, u_1, v_1, w_1, $\rho_1 = 1.0$.

$$a_1^2 = \rho_1^{\gamma-1}/M_\infty^2$$

$$M_s^2 = \frac{2}{(\gamma-1)} \frac{\left(\rho_2^{\gamma+1} - \rho_2^2\right)}{\left(\rho_2^2 - 1\right)}$$

$$U_{1N} = M_s\, a_1$$

As an example, η_x is assumed unknown

$$A = u_1^2 - U_{1N}^2$$

$$B = u_1(v_1\eta_y + w_1\eta_z)$$

$$C = (v_1^2 - U_{1N}^2)\eta_y^2 + (w_1^2 - U_{1N}^2)\eta_z^2 + 2v_1 w_1 \eta_y \eta_z$$

$$\eta_x = (-B \pm \sqrt{B^2 - AC})/A \qquad (5.20)$$

(The particular root to be calculated must be specified)

$$U_{1N} = (u_1\eta_x + v_1\eta_y + w_1\eta_z)/\sqrt{\eta_x^2 + \eta_y^2 + \eta_z^2}$$

$$u_2 = u_1 + U_{1N}\left(\frac{1}{\rho_2} - 1\right) \frac{\eta_x}{\sqrt{\eta_x^2 + \eta_y^2 + \eta_z^2}}$$

$$v_2 = v_1 + U_{1N}\left(\frac{1}{\rho_2} - 1\right) \frac{\eta_y}{\sqrt{\eta_x^2 + \eta_y^2 + \eta_z^2}}$$

$$w_2 = w_1 + U_{1N}\left(\frac{1}{\rho_2} - 1\right) \frac{\eta_z}{\sqrt{\eta_x^2 + \eta_y^2 + \eta_z^2}}$$

The vector approach which solves Eq. (5.11) has both advantages and disadvantages. The main advantage is that it is casted in a convenient conservative form which is readily adaptable to any hyperbolic finite difference scheme, especially the MacCormack method. The disadvantages are that one must store ρ, u, v and w at each grid point, which

means enormous storage requirements for a three-dimensional problem (Euler solvers require even more storage than the current full potential vector approach due to the addition of the more variable pressure), and the decoding process which involves solving a polynomial is very time consuming.

In order to alleviate the above mentioned disadvantages of the vector approach, an alternate method for solving the conservative form of the full potential equation is proposed in the next section.

5.2 SCALAR APPROACH

The method to be described in this section is termed scalar approach because the objective of the method is to solve for the scalar velocity potential ϕ rather than for u, v, w and ρ as in the vector approach. Such a method would eliminate the decoding process described in Section 5.1.1 and also substantially reduce the storage requirement because only one variable, ϕ, need be stored at each grid point. Both these factors should contribute toward increasing the computational efficiency and speed. In what follows, an implicit marching scheme utilizing a mathematically sound density linearization method which solves for the scalar velocity potential ϕ is described.

Referring to Fig. 5.2, let us assume that the ϕ information is given at all points in planes i, i-1, and i-2. The objective is to compute the ϕ information in plane i+1 by solving Eq. (5.1).

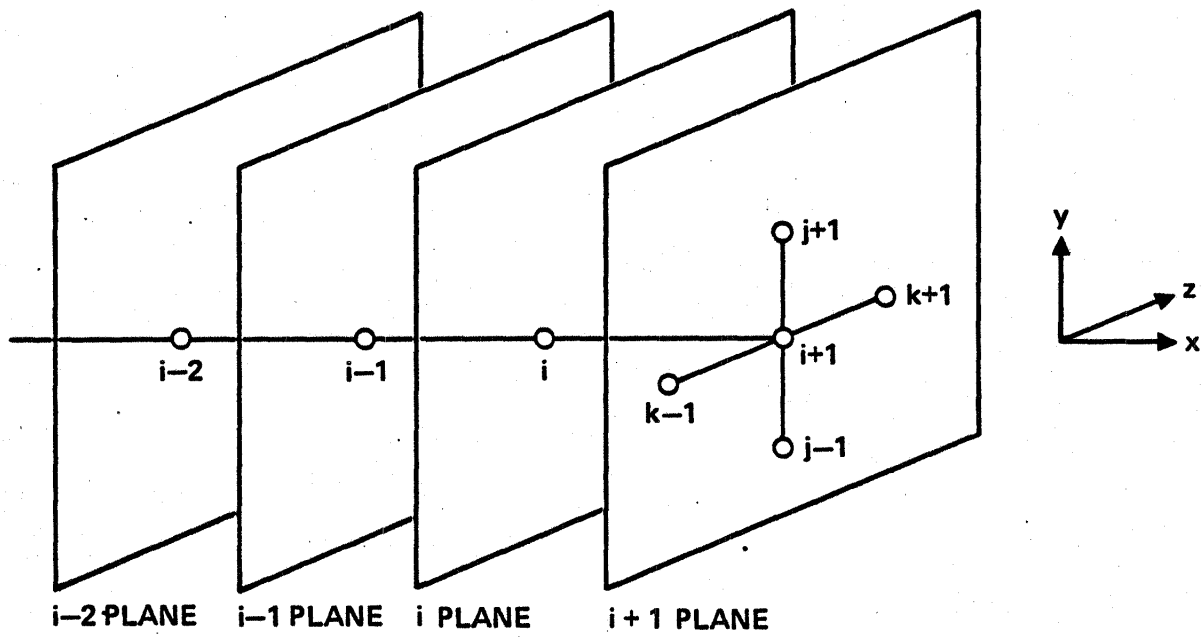

Figure 5.2. Implicit Computational Molecule

The implicit finite differenced form of Eq. (5.1) can be written as

$$\left[\frac{\rho_{i+1,j,k}u_{i+1,j,k} - \rho_{i,j,k}u_{i,j,k}}{\Delta x}\right] + \left[\frac{\rho_{i+1,j+\frac{1}{2},k}v_{i+1,j+\frac{1}{2},k} - \rho_{i+1,j-\frac{1}{2},k}v_{i+1,j-\frac{1}{2},k}}{\Delta y}\right] + \left[\frac{\rho_{i+1,j,k+\frac{1}{2}}w_{i+1,j,k+\frac{1}{2}} - \rho_{i+1,j,k-\frac{1}{2}}w_{i+1,j,k-\frac{1}{2}}}{\Delta z}\right] = 0 . \tag{5.21}$$

In Eq. (5.21), the flow quantities like density ρ and velocity components u, v, and w appear at the i+1 level, which makes it difficult to solve for ϕ at i+1 without introducing some kind of a linearization. Since ρ is a complicated function of ϕ, the logical variable to linearize is density.

Consider the first bracketed term in Eq. (5.21) which represents the mass flux balance in the x-direction. To write this in terms of ϕ_{i+1} values, let us linearize ρ_{i+1} in terms of ρ_i and ρ_i in terms of ρ_{i-1}. To maintain the conservation law form both ρ_{i+1} and ρ_i have to be linearized. Thus,

$$\rho_{i+1,j,k}u_{i+1,j,k} \doteq \left\{\rho_{i,j,k} + \left(\frac{\partial \rho}{\partial x}\Delta x\right)_{i,j,k} + \cdots\right\} u_{i+1,\,j,k} \tag{5.22}$$

where

$$\frac{\partial \rho}{\partial x} = -\rho^{2-\gamma}M_\infty^2(uu_x + vv_x + ww_x) . \tag{5.23}$$

Substituting Eq. (5.23) into Eq. (5.22) and rearranging the terms results in the following. For convenience, the subscripts j and k are suppressed.

$$\begin{aligned}\rho_{i+1}u_{i+1} \doteq & \left[\rho_i - \rho_i^{2-\gamma}M_\infty^2 u_i^2\right] u_{i+1} \\ & + \rho_i^{2-\gamma}M_\infty^2(u_i^3 + u_i v_i^2 + u_i w_i^2) \\ & - \rho_i^{2-\gamma}M_\infty^2 u_i v_i v_{i+1} - \rho_i^{2-\gamma}M_\infty^2 u_i w_i w_{i+1}\end{aligned} \tag{5.24}$$

where

$$u_{i+1,j,k} = \left(\frac{\phi_{i+1} - \phi_i}{\Delta x}\right)_{j,k} \quad ; \quad \text{backward differenced}$$

$$\left.\begin{aligned} v_{i+1,j,k} &= \frac{\phi_{i+1,j+1,k} - \phi_{i+1,j-1,k}}{2\Delta y} \\ w_{i+1,j,k} &= \frac{\phi_{i+1,j,k+1} - \phi_{i+1,j,k-1}}{2\Delta z} \end{aligned}\right\} \quad \text{central differenced} \tag{5.25}$$

Similarly, expanding $\rho_{i,j.k}$ about $\rho_{i-1,j,k}$ (even through $\rho_{i,j,k}$ is known, to maintain conservative differencing it has to be expanded about $\rho_{i-1,j,k}$), we can write (suppressing j and k indices)

$$\rho_{i,j,k}u_{i,j,k} \doteq \left[\rho_{i-1} - \rho_{i-1}^{2-\gamma}M_\infty^2 u_{i-1}^2\right]u_i$$

$$+ \rho_{i-1}^{2-\gamma}M_\infty^2(u_{i-1}^3 + u_{i-1}v_{i-1}^2 + u_{i-1}w_{i-1}^2) \qquad (5.26)$$

$$- \rho_{i-1}^{2-\gamma}M_\infty^2 u_{i-1}v_{i-1}v_i$$

$$- \rho_{i-1}^{2-\gamma}M_\infty^2 u_{i-1}w_{i-1}w_i = f_i$$

Combining Eqs. (5.24) and (5.26), one can write the first term in Eq. (5.1) as

$$\frac{\partial \rho u}{\partial x} \doteq \frac{1}{\Delta x}\left[(\rho_i - \rho_i^{2-\gamma}M_\infty^2 u_i^2)u_{i+1} - \rho_i^{2-\gamma}M_\infty^2 u_i v_i v_{i+1}\right.$$

$$\left. - \rho_i^{2-\gamma}M_\infty^2 u_i w_i w_{i+1} - f_i + \rho_i^{2-\gamma}M_\infty^2 u_i(u_i^2 + v_i^2 + w_i^2)\right] . \qquad (5.27)$$

In Eq. (5.27), only the velocities u, v, and w appear at the unknown i+1 level. The density is linearized in such a way (using Eqs. (5.22) and (5.23) that it appears only at the known i and i-1 levels. Substituting for u, v, and w in terms of the velocity potential ϕ from Eq. (5.25), and defining a differential velocity potential $\Delta\phi$ such that $\Delta\phi = \phi_{i+1,j,k} - \phi_{i,j,k}$, Eq. (5.27) can be finally written into delta form as

$$\frac{\partial(\rho u)}{\partial x} = \frac{1}{\Delta x^2}\left\{\rho_i - \rho_i^{2-\gamma M_\infty^2 u_i^2}\right\}\Delta\phi - \frac{1}{\Delta x}\,\rho_i^{2-\gamma M_\infty^2 u_i v_i}\,\frac{\partial}{\partial y}\,\Delta\phi$$

$$- \frac{1}{\Delta x}\,\rho_i^{2-\gamma M_\infty^2 u_i w_i}\,\frac{\partial}{\partial z}\,\Delta\phi - \frac{1}{\Delta x}\left\{f_i - \rho_i^{2-\gamma M_\infty^2 u_i^3}\right\} . \qquad (5.28$$

There are some interesting physics featured in Eq. (5.28) which will be discussed later. Now, consider the second term in Eq. (5.1) whose finite differenced form is given by the second bracketed term in Eq. (5.21). Here again, both the density and velocity v appear at the i+1 level and some kind of a density linearization is essential to solve for ϕ at the i+1 level. A simple linearization of the type

$$\left.\begin{aligned} \rho_{i+1,j+\frac{1}{2},k} &\doteq \rho_{i,j+\frac{1}{2},k} \\ \rho_{i+1,j-\frac{1}{2},k} &\doteq \rho_{i,j-\frac{1}{2},k} \end{aligned}\right\} \qquad (5.29)$$

is sufficient for the y-derivative treatment in the Cartesian framework since the velocity component v is usually subsonic for a predominantly supersonic flow in the x-direction. If the v component does go from subsonic to supersonic or vice versa, then the density linearization given by Eq. (5.29) will have to be modified to a slightly complicated form, which will not be discussed here. Using Eq. (5.29), the second term in Eq. (5.1) or Eq. (5.21) can be written in the delta form as

$$\frac{\partial \rho v}{\partial y} = \frac{\partial}{\partial y} \rho_{i+1} \frac{\partial}{\partial y} \phi_{i+1} \doteq \frac{\partial}{\partial y} \rho_i \frac{\partial}{\partial y} (\phi_{i+1} - \phi_i + \phi_i)$$

$$= \frac{\partial}{\partial y} \rho_i \frac{\partial}{\partial y} \Delta\phi + \frac{\partial}{\partial y} (\rho_i v_i) \ . \tag{5.30}$$

Similarly, the z-derivative term in Eq. (5.1) can be linearized and written as

$$\frac{\partial \rho w}{\partial z} \doteq \frac{\partial}{\partial z} \rho_i \frac{\partial}{\partial z} \Delta\phi + \frac{\partial}{\partial z} (\rho_i w_i) \ . \tag{5.31}$$

Combining Eqs. (5.28), (5.30), and (5.31), we have the final density linearized form of the full potential equation.

$$\frac{\beta}{\Delta x^2} \Delta\phi - \frac{1}{\Delta x} \rho_i^{2-\gamma} M_\infty^2 u_i v_i \frac{\partial}{\partial y} \Delta\phi - \frac{1}{\Delta x} \rho_i^{2-\gamma} M_\infty^2 u_i w_i \frac{\partial}{\partial z} \Delta\phi$$

$$+ \frac{\partial}{\partial y} \rho_i \frac{\partial}{\partial y} \Delta\phi + \frac{\partial}{\partial z} \rho_i \frac{\partial}{\partial z} \Delta\phi = R_i \tag{5.32}$$

where

$$\beta = \rho_i - \rho_i^{2-\gamma} M_\infty^2 u_i^2$$

$$R_i = \frac{1}{\Delta x} \left\{ f_i - \rho_i^{2-\gamma} M_\infty^2 u_i^3 \right\} - \frac{\partial}{\partial y} (\rho_i v_i) - \frac{\partial}{\partial z} (\rho_i w_i) \ .$$

In Eq (5.32), both the y and z derivative terms appear in an implicit manner which makes it difficult to solve without some approximations to the left hand side. Factoring the left hand side into (x,y) terms and (x,z) terms for computational implementation, we get

$$\underbrace{\left(\frac{\beta}{\Delta x^2} - \frac{1}{\Delta x}\rho_i^{2-\gamma}M_\infty^2 u_i w_i \frac{\partial}{\partial z} + \frac{\partial}{\partial z}\rho_i \frac{\partial}{\partial z}\right)}_{A}\underbrace{\left(\frac{\beta}{\Delta x^2} - \frac{1}{\Delta x}\rho_i^{2-\gamma}M_\infty^2 u_i v_i \frac{\partial}{\partial y} + \frac{\partial}{\partial y}\rho_i \frac{\partial}{\partial y}\right)}_{B}\Delta\phi = R_i \tag{5.33}$$

In the above equation A and B are operators where the operator A gives rise to an implicit molecule in the x-z plane, while B results in an implicit molecule in the x-y plane. The solution procedure for Eq. (5.33) is twofold. Define $\Delta\phi^* = B\Delta\phi$ and then perform the following:

$$\left.\begin{aligned} A\Delta\phi^* &= R_i \\ B\Delta\phi &= \Delta\phi^* \\ \phi_{i+1,j,k} &= \phi_{i,j,k} + \Delta\phi \end{aligned}\right\} . \tag{5.34}$$

The implicit operator A when written down results in a tridiagonal form as shown below.

$$\begin{bmatrix} & & \\ a & b & c \\ & & \end{bmatrix} \begin{bmatrix} \\ \Delta\phi^* \\ \\ \end{bmatrix} = \begin{bmatrix} \\ R_i \\ \\ \end{bmatrix} . \tag{5.35}$$

For the solution procedure to converge, it is necessary and sufficient that the above tridiagonal matrix possess diagonal dominance such that

$$|b| \geq |a| + |c| . \tag{5.36}$$

The diagonal term b looks like

$$b = \frac{\beta}{\Delta x^2} - \left(\frac{\rho_{i,j,k+\frac{1}{2}} + \rho_{i,j,k-\frac{1}{2}}}{\Delta z^2} \right) . \tag{5.37}$$

In order to ensure diagonal dominance the term $\beta/\Delta x^2$ has to be negative. Let us go back and review the term β with the physics of the problem in mind.

$$\beta = \rho_i - \rho_i^{2-\gamma} M_\infty^2 u_i^2 . \tag{5.38}$$

Also, the density is related to the speed of sound and Mach number through

$$\rho_i^{\gamma-1} = a_i^2 M_\infty^2 \,. \tag{5.39}$$

where a_i is the local speed of sound.

Substituting Eq. (5.39) into Eq. (5.38) we get

$$\beta = \rho_i \left(1 - \frac{u_i^2}{a_i^2}\right). \tag{5.40}$$

If we assume the flow is supersonic in the marching direction x, then it implies $u_i > a_i$, which means,

$$\left(1 - \frac{u_i^2}{a_i^2}\right) < 0 \tag{5.41}$$

or

$$\beta < 0 \,.$$

This diagonal dominance property was achieved only through the particular form of the density linearization assumed in Eqs. (5.22) and (5.23). If we had assumed at that point that $\rho_{i+1,j,k} \doteq \rho_{i,j,k}$ without the second term $\left(\frac{\partial \rho}{\partial x}\right)_{i,j,k}$, then the final expression for β would have resulted in $\beta = \rho_i$ which would always be positive, and diagonal dominance is not ensured. Thus, the form of density linearization is very critical for convergence of the solution procedure.

5.2.1 Arbitrary Coordinate System

The entire analysis described in Section 5.2 assumed a Cartesian framework where it is convenient to explain the density linearization concept and also simple to construct a computer program to test the concepts. However, for the treatment of wing-body configurations, a body-fitted coordinate transformation is essential for application of body boundary conditions. In this section, a brief introduction is made for the inclusion of a coordinate transformation into Eq. (5.1) and the associated density linearization procedure.

Considering the general transformation given by Eq. (5.10), one can write Eq. (5.1) in the form

$$\frac{\partial\left(\frac{\rho U}{J}\right)}{\partial\sigma} + \frac{\partial\left(\frac{\rho V}{J}\right)}{\partial\xi} + \frac{\partial\left(\frac{\rho W}{J}\right)}{\partial\eta} = 0 \tag{5.42}$$

where

$$\left.\begin{aligned} U &= u\sigma_x + v\sigma_y + w\sigma_z = A_1\phi_\sigma + A_2\phi_\xi + A_3\phi_\eta \\ V &= u\xi_x + v\xi_y + w\xi_z = A_4\phi_\sigma + A_5\phi_\xi + A_6\phi_\eta \\ W &= u\eta_x + v\eta_y + w\eta_z = A_7\phi_\sigma + A_8\phi_\xi + A_9\phi_\eta \\ \rho^{\gamma-1} &= \left[1 - \frac{\gamma-1}{2} M_\infty^2 (U\phi_\sigma + V\phi_\xi + W\phi_\eta - 1)\right] \end{aligned}\right\} \tag{5.43}$$

$$
\left.
\begin{aligned}
A_1 &= \sigma_x^2 + \sigma_y^2 + \sigma_z^2 \\
A_2 &= \sigma_x \xi_x + \sigma_y \xi_y + \sigma_z \xi_z \\
A_3 &= \sigma_x \eta_x + \sigma_y \eta_y + \sigma_z \eta_z \\
A_4 &= A_2 \\
A_5 &= \xi_x^2 + \xi_y^2 + \xi_z^2 \\
A_6 &= \xi_x \eta_x + \xi_y \eta_y + \xi_z \eta_z \\
A_7 &= A_3 \\
A_8 &= A_6 \\
A_9 &= \eta_x^2 + \eta_y^2 + \eta_z^2
\end{aligned}
\right\} \qquad (5.43)
$$

In Eq. (5.42), the direction σ can be considered as the marching direction (time-like hyperbolic direction), provided the projection of the velocity in the direction normal to the constant $\dot{\sigma}$ line/surface is supersonic. This is illustrated in Fig. 5.3 and the verification of the above statement will become clear once the density linearization is introduced into the first term of Eq. (5.42).

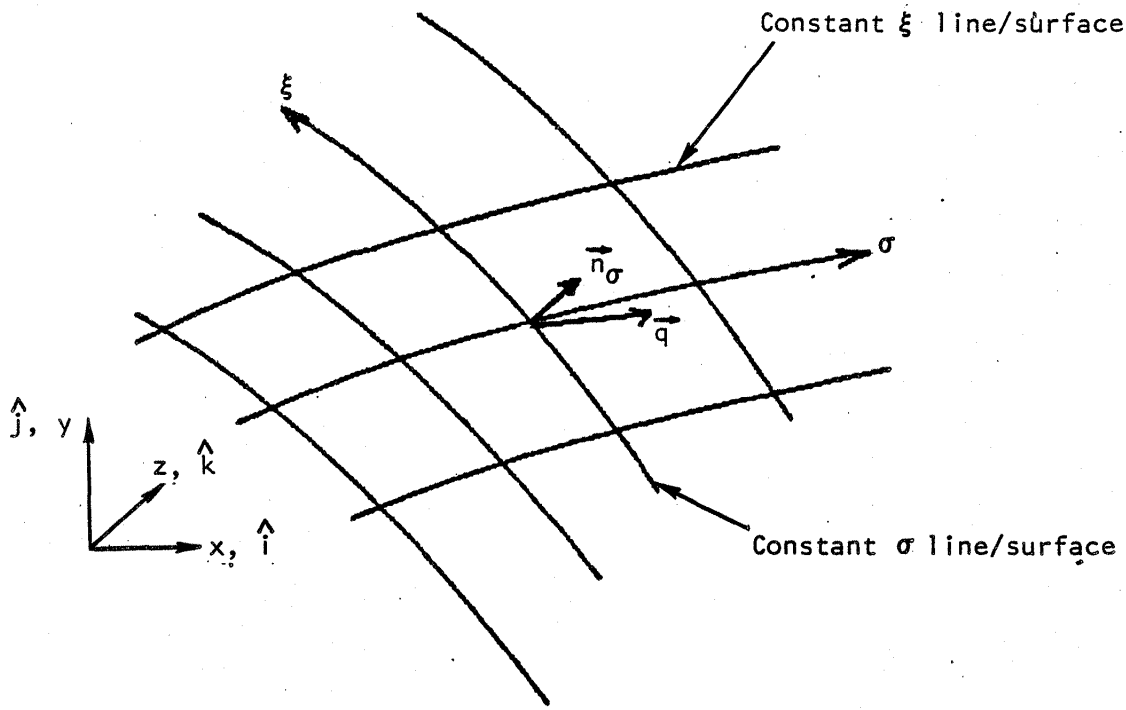

$$\vec{n}_\sigma = \frac{\sigma_x \hat{i} + \sigma_y \hat{j} + \sigma_z \hat{k}}{\sqrt{\sigma_x^2 + \sigma_y^2 + \sigma_z^2}}$$

$\vec{n}_\sigma$ ~ unit normal vector

$\vec{q}$ ~ velocity vector

$$\vec{q} \cdot \vec{n}_\sigma = \frac{u\sigma_x + v\sigma_y + w\sigma_z}{\sqrt{\sigma_x^2 + \sigma_y^2 + \sigma_z^2}} = \frac{U}{\sqrt{\sigma_x^2 + \sigma_y^2 + \sigma_z^2}} = \frac{A_1\phi_\sigma + A_2\phi_\xi + A_3\phi_\eta}{\sqrt{\sigma_x^2 + \sigma_y^2 + \sigma_z^2}}$$

For σ to be the marching direction $(\vec{q} \cdot \vec{n}_\sigma) > a$
where a is the local speed of sound.

Figure 5.3. - Definition of a time-like marching direction.

Consider the first term in Eq. (5.42). The objective now is to linearize the density term ρ in such a way we can not only show the requirement for σ to be the marching direction but also be able to solve for the velocity potential ϕ. Let ρ be expanded about ρ_0 where ρ_0 is some neighboring known state.

$$\rho = \rho_0 + \left(\frac{\partial \rho}{\partial \sigma}\right)_0 \Delta\sigma + \cdots \tag{5.44}$$

where

$$\frac{\partial \rho}{\partial \sigma} = - \frac{\rho_0}{a_0^2} \left\{ U_0 \frac{\partial}{\partial \sigma} \phi_\sigma + V_0 \frac{\partial}{\partial \sigma} \phi_\xi + W_0 \frac{\partial}{\partial \sigma} \phi_\eta \right\} .$$

Using Eq. (5.44) we can write

$$\frac{\partial \left(\frac{\rho U}{J}\right)}{\partial \sigma} = \frac{\partial}{\partial \sigma} \left\{ \left[\rho_0 - \frac{\rho_0}{a_0^2} \left\{ U_0 \phi_\sigma + V_0 \phi_\xi + W_0 \phi_\eta + f_0 \right\} \right] \frac{U}{J} \right\} \tag{5.45}$$

where

$$f_0 = U_0 \left(\phi_\sigma\right)_0 + V_0 \left(\phi_\xi\right)_0 + W_0 \left(\phi_\eta\right)_0$$

$$\frac{\partial \left(\frac{\rho U}{J}\right)}{\partial \sigma} \doteq \frac{\partial \left(\rho_0 \frac{U}{J}\right)}{\partial \sigma} - \frac{\partial}{\partial \sigma} \left(\frac{1}{J} \frac{\rho_0}{a_0^2} \left\{ U_0^2 \phi_\sigma + U_0 V_0 \phi_\xi + W_0 U_0 \phi_\eta + f_0 U_0 \right\} \right) . \tag{5.46}$$

Substituting for U in terms of A_1, A_2 and A_3, and rewriting Eq. (5.46), we get

$$\frac{\partial\left(\frac{\rho U}{J}\right)}{\partial\sigma} \doteq \frac{\partial}{\partial\sigma}\left[\frac{A_1\rho_0}{J}\left\{1 - \frac{U_0^2}{A_1 a_0^2}\right\}\phi_\sigma\right] + \frac{\partial}{\partial\sigma}\left[\frac{\rho_0}{J}\left(\left\{A_2 - \frac{U_0V_0}{a_0^2}\right\}\phi_\xi + \left\{A_3 - \frac{W_0U_0}{a_0^2}\right\}\phi_\eta - \frac{f_0U_0}{a_0^2}\right)\right] \tag{5.47}$$

where

$$\left.\begin{aligned} \frac{\partial(\,)}{\partial\sigma} &= \frac{(\,)_{i+1,j,k} - (\,)_{i,j,k}}{\Delta\sigma} \quad ; \text{ backward differenced} \\ \left.\begin{aligned} \frac{\partial(\,)}{\partial\xi} &= \frac{(\,)_{i+1,j+1,k} - (\,)_{i+1,j-1,k}}{2\Delta\xi} \\ \frac{\partial(\,)}{\partial\eta} &= \frac{(\,)_{i+1,j,k+1} - (\,)_{i+1,j,k-1}}{2\Delta\eta} \end{aligned}\right\}; \text{ central differenced} \end{aligned}\right\} \tag{5.48}$$

To ensure diagonal dominance for stability, the term

$$\left(1 - \frac{U_0^2}{A_1 a_0^2}\right)$$

appearing in Eq. (5.47) has to be negative. This implies (if backward differencing is used in σ)

$$\frac{U_0^2}{A_1} > a_0^2$$

or ; for stability . (5.49)

$$\frac{U_0}{\sqrt{A_1}} > a_0$$

The quantity $U_0/\sqrt{A_1}$ is nothing but the projection of the velocity vector $\vec{q}$ in the direction normal to the constant σ surface as shown in Fig. 5.3. Thus, it is verified that for σ to be the marching direction, $U/\sqrt{A_1}$ has to be supersonic. The Cartesian framework described in Section 5.2 (Eq. (5.27)) is contained in Eq. (5.47) as a special case (set σ=x; ξ=y; η=z; A_1=1; $A_2 = A_3 = 0$; J=1; U_0=u_0; V_0=v_0; W_0=w_0).

The formulation for the scalar approach in the transformed coordinate system σ,ξ,η is at present in the conceptual stage as far as the treatment of $\left(\frac{\rho v}{J}\right)_\xi$ and $\left(\frac{\rho w}{J}\right)_\eta$ terms in Eq. (5.42). Results from the scalar approach to be presented in this report are based on the Cartesian system (Eq. (5.1)).

6.0 RESULTS

6.1 SECOND ORDER COMPARISONS

Comparisons were performed to determine the success of the proposed second order analysis technique in prediction of surface pressures, forces, and moments. The following sections present comparisons between first and second order analysis, experimental data, and higher order numerical calculations.

6.1.1 Wing Alone

Figures 6.1.1 through 6.1.3 present first and second order results for wing alone cases. The predictions are based on using perturbation velocities obtained by placing the free stream at angle of attack. The comparisons indicate that even for wings with subsonic edges and in cases where the flow was far from two dimensional, the predictions were quite good. The integrated lift and moment calculation shown in figure 6.1.3 demonstrates a substantial improvement in the aerodynamic center prediction for a wing with a subsonic edge. Reference 1 presents similar results for a wing with a supersonic leading edge based on a source volume method. The present analysis gives virtually the same answer.

6.1.2 Bodies of Revolution

The pressures and velocities on bodies of revolution were computed by combining a first or second order axial solution with a first order cross flow solution. Cone thickness and angle of attack comparisons between hybrid second order analysis and the complete Euler equations, figures 6.1.4 through 6.1.6, demonstrates that a second order analysis can yield considerable improvement over first order results even for values of $M\delta$ near 1. The results for a non-lifting parabolic body of revolution, presented in figure 6.1.7, show that the difference between a first and second order analysis is greatest in regions of highest flow deflection angle near the nose and tail as would be expected .

Figures 6.1.4 and 6.1.5, demonstrate that the second order velocities computed for axial flow past cones compares very favorably with the exact solutions. The second order solution appears to be accurate to values of $M\delta$ approaching 1. Figure 6.1.6 show how the isentropic pressure coefficient formula, when combined with the accurate velocity predictions result in good prediction of the pressure coefficients for lifting cones.

Results for $M = 6$ flow past the body shown in figure 6.1.8 are presented in figure 6.1.9. For analysis purposes the nose region of the body has to be modified to avoid slopes which exceed the Mach angle. A conical forebody extension having a slope slightly less than the Mach angle was used for this purpose. In the nose region, where the values of $M\delta$ were large, differences between the analysis and the experimental data are noticeable. The greater slopes present on some bodies can restrict regions which may be usefully analyzed.

6.1.3 Delta Wing-Body

Figure 6.1.10 present results for the pressure coefficient calculation for flow past the wing-body combination shown in figure 6.1.8. For most regions on the wing, a comparison with the experimental data is reasonably good.

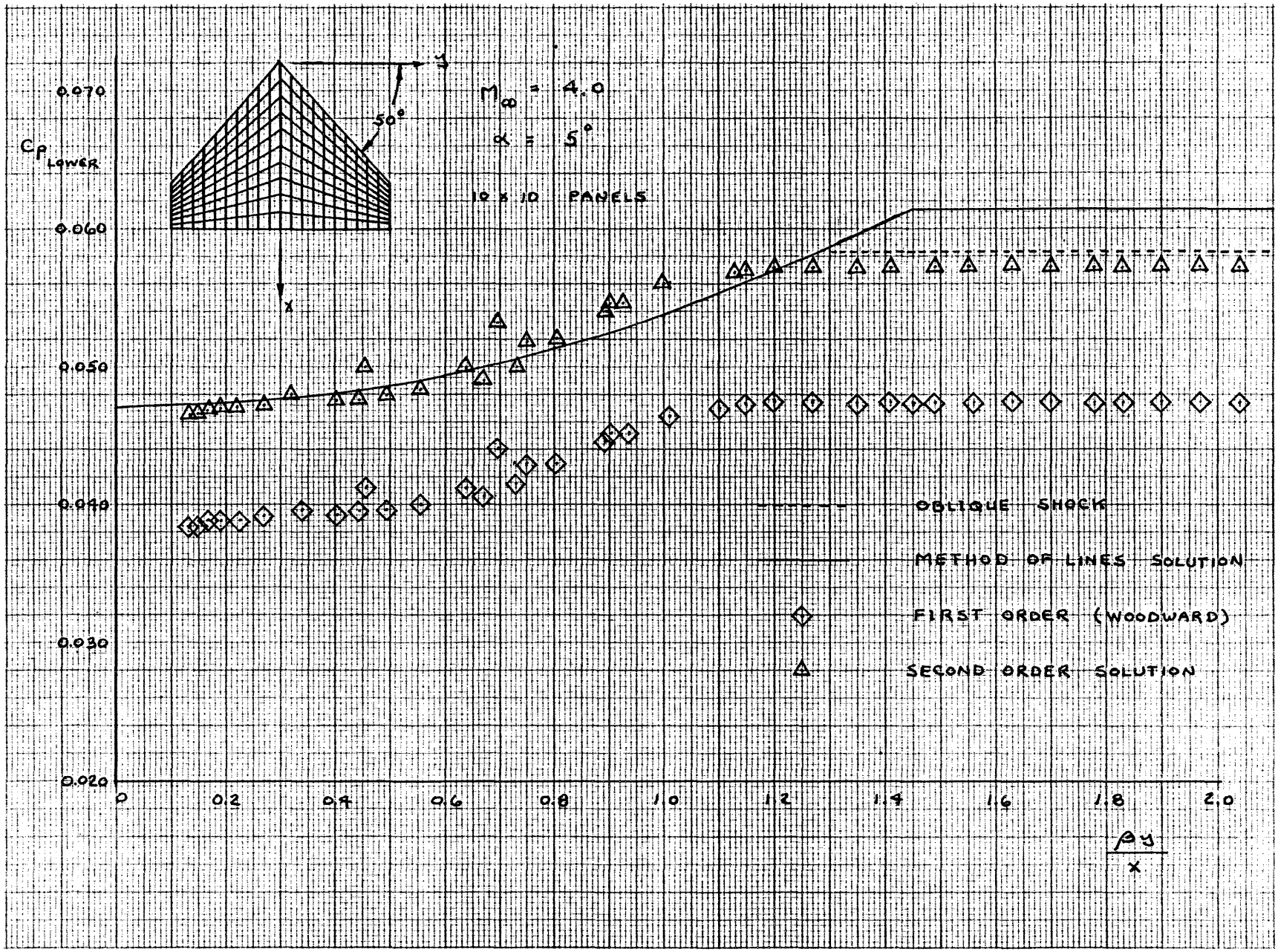

Figure 6.1.1. Comparison of Measured and Predicted Compression
ssu for upe ic e D Wi

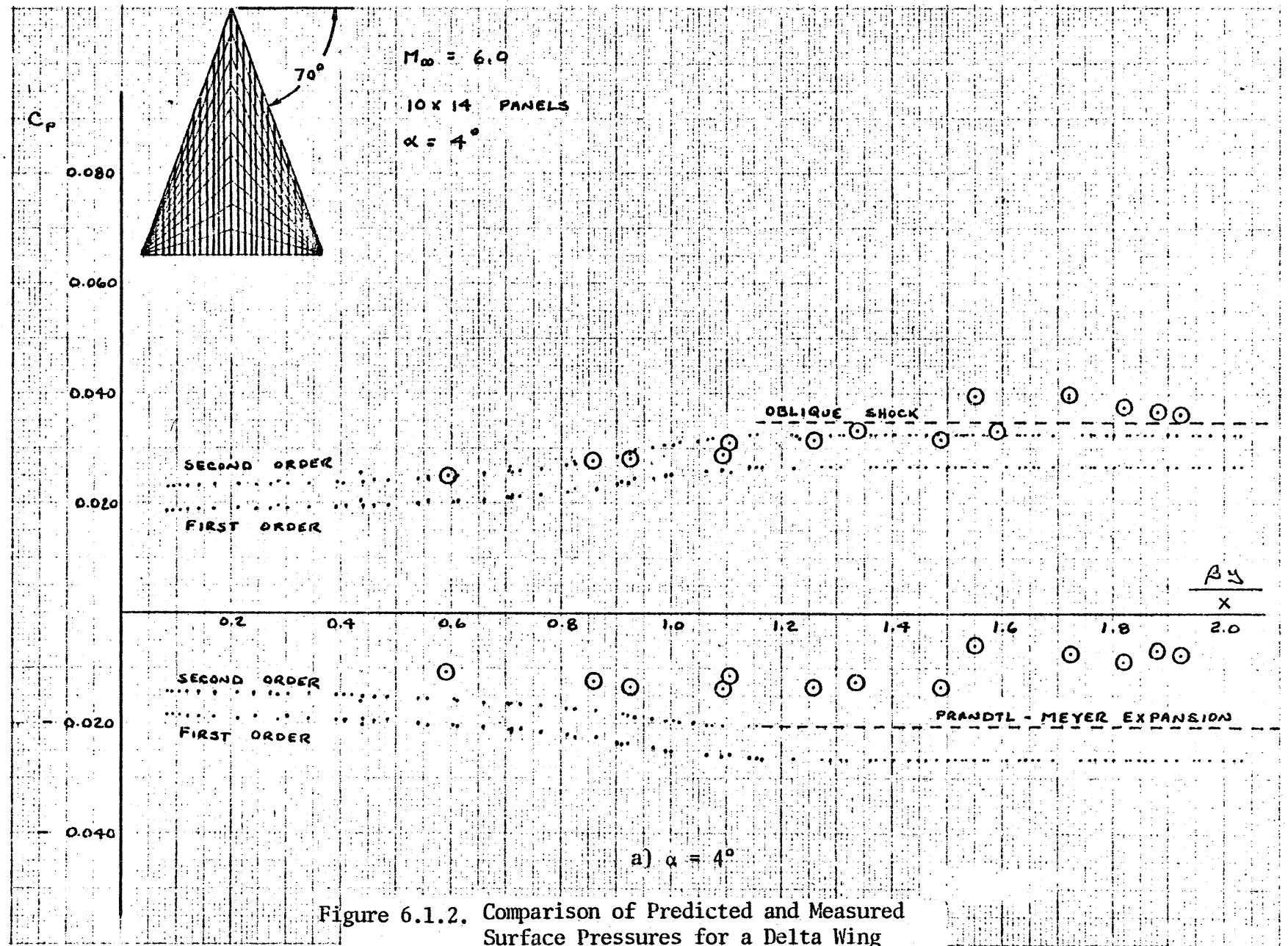

a) α = 4°

Figure 6.1.2. Comparison of Predicted and Measured Surface Pressures for a Delta Wing at M = 6

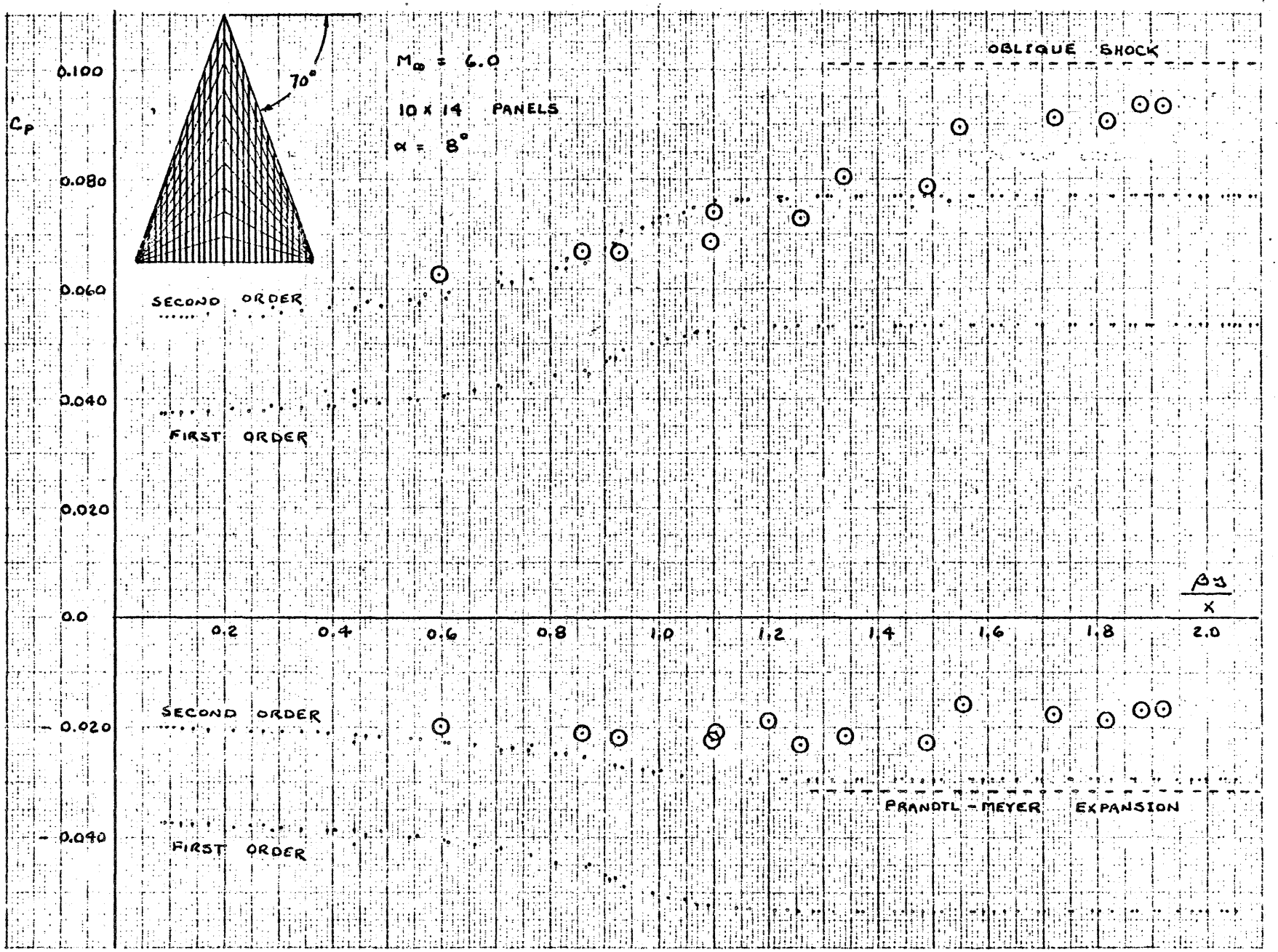

Figure 6.1.2, Concluded b) α = 8°

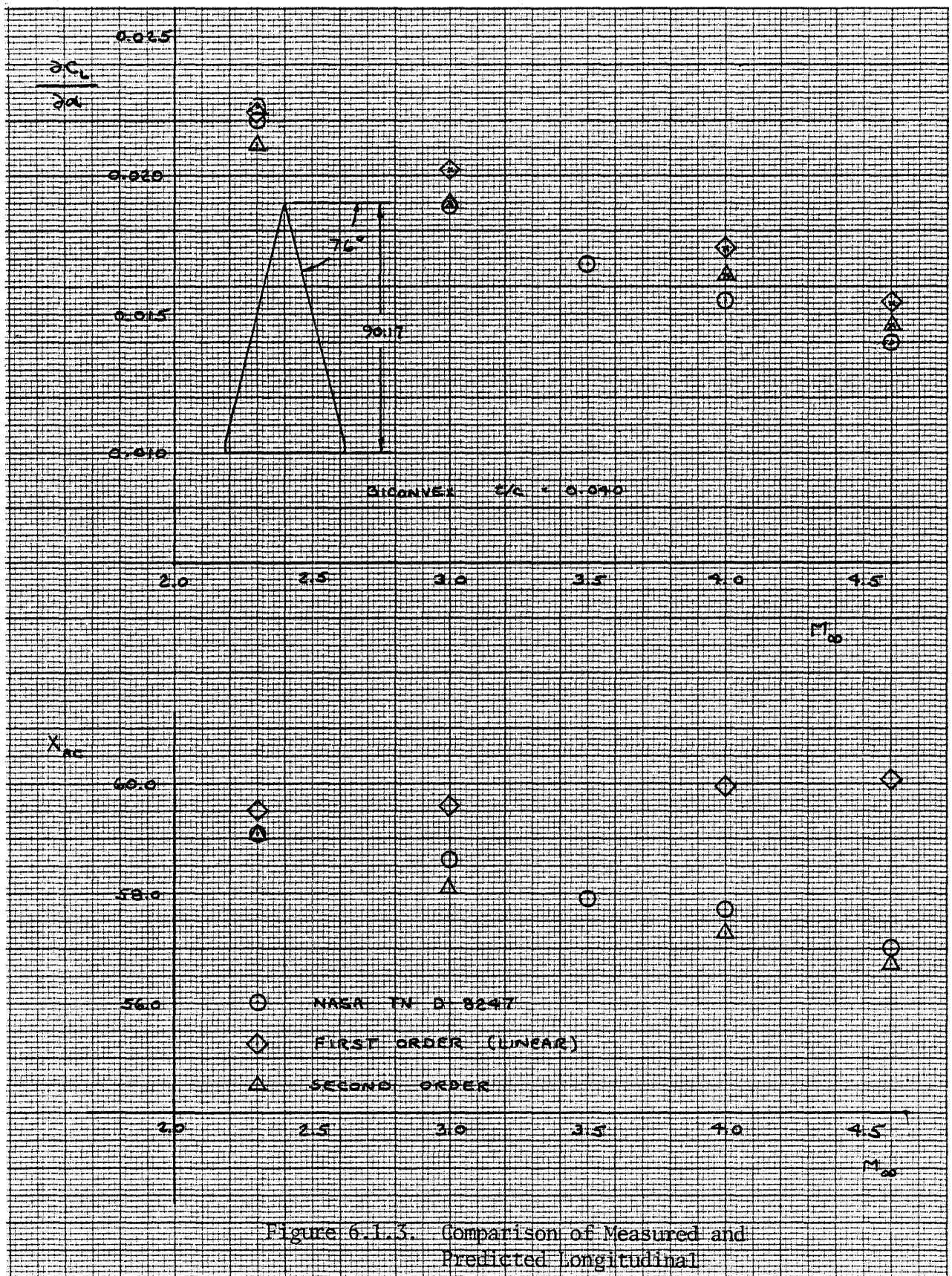

Figure 6.1.3. Comparison of Measured and Predicted Longitudinal Characteristics for a Subsonic Edge Delta Wing

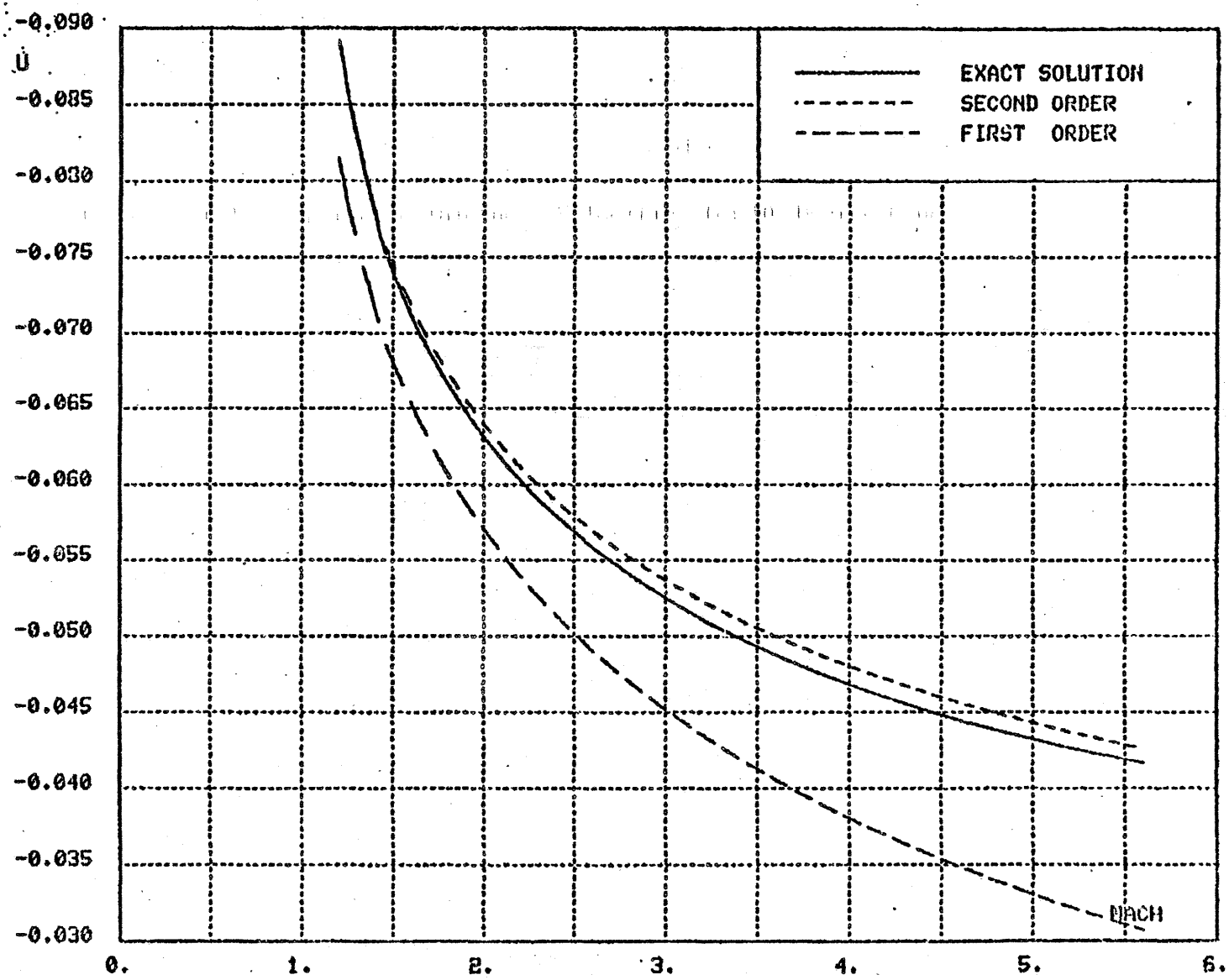

a) Axial Component

Figure 6.1.4. Supersonic Thickness Velocities for 10 Degree Cone

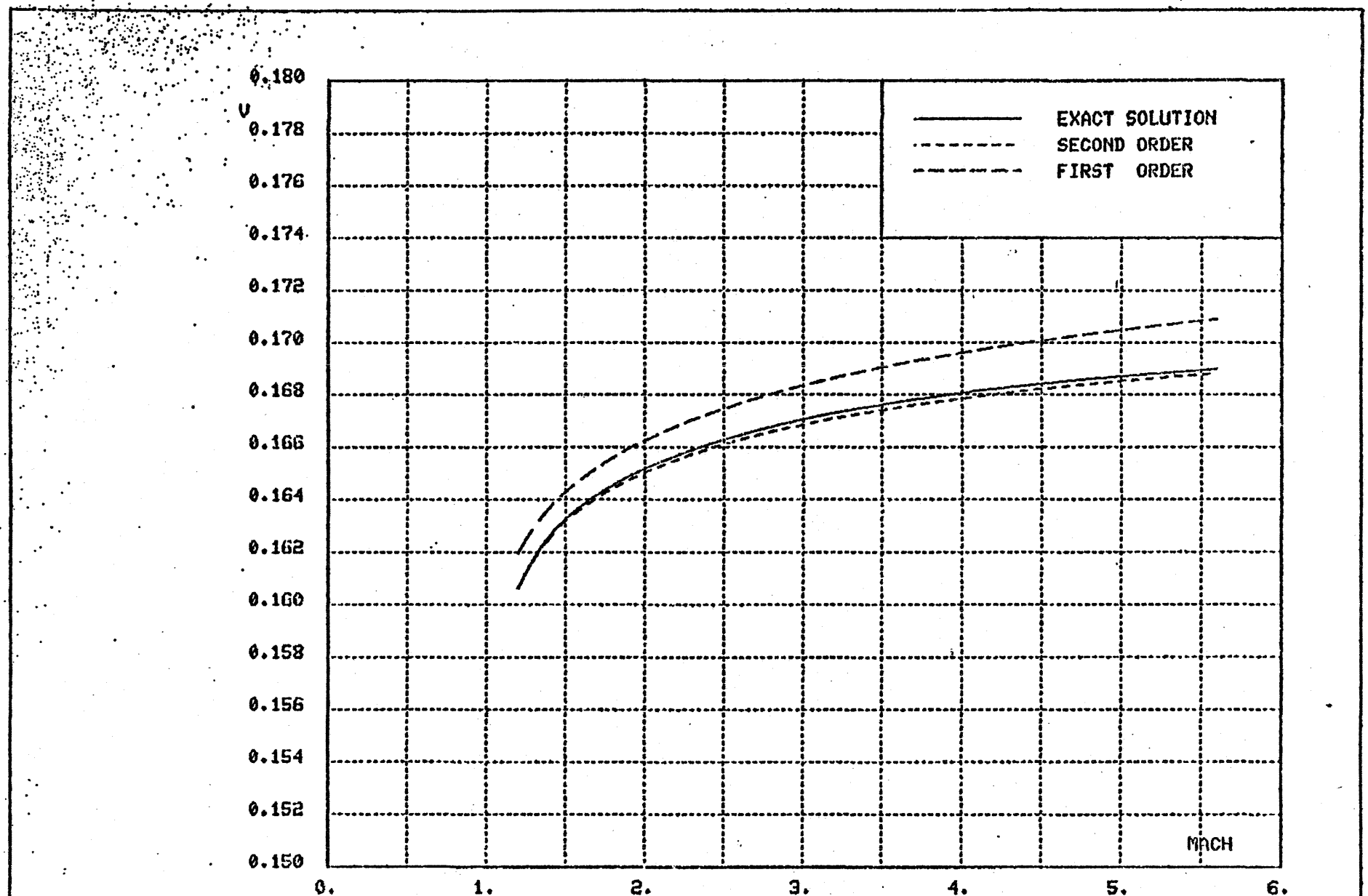

b) Radial Component

Figure 6.1.4. Completed

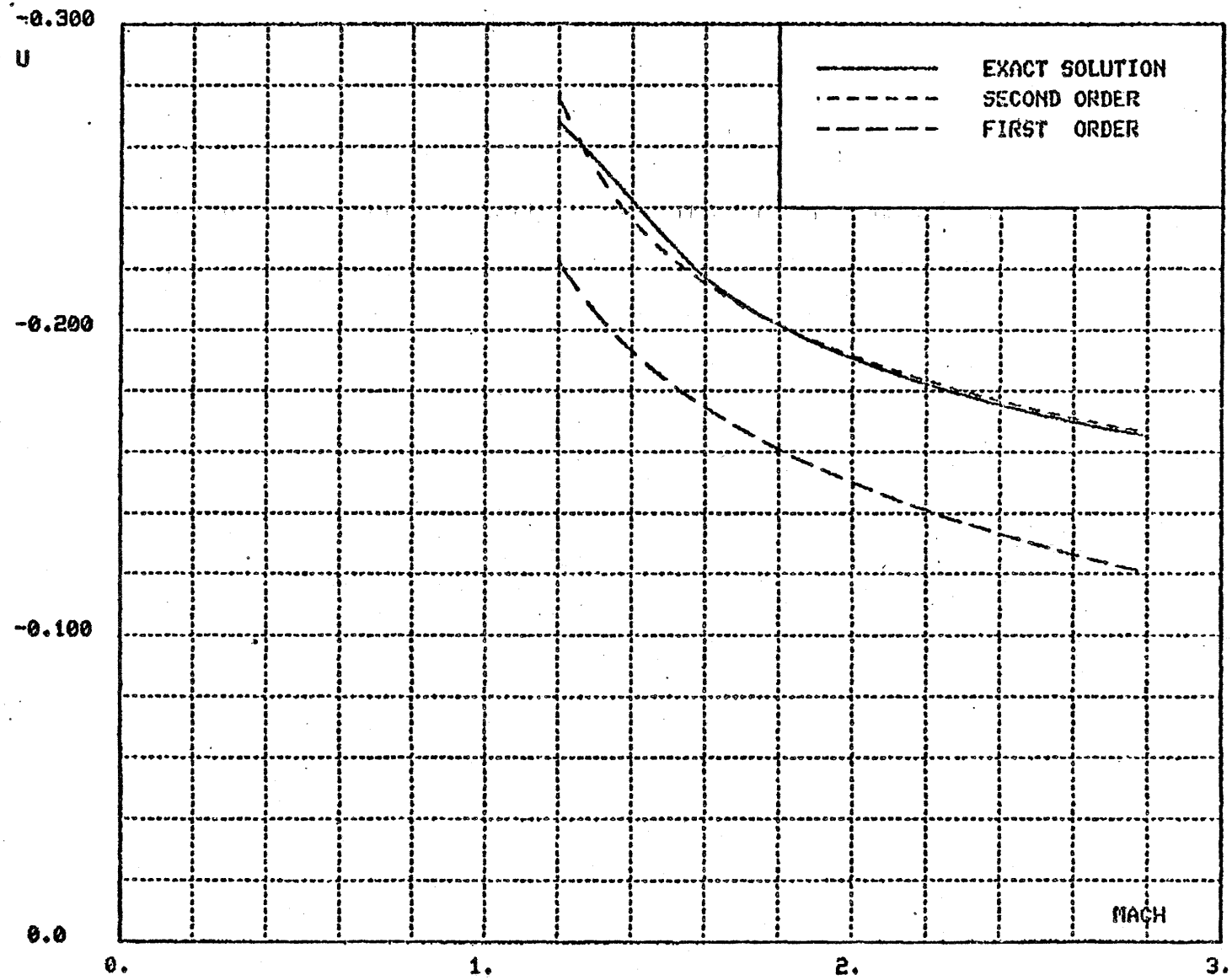

a) Axial Component

Figure 6.1.5. Supersonic Thickness Velocities for a 20 Degree Cone

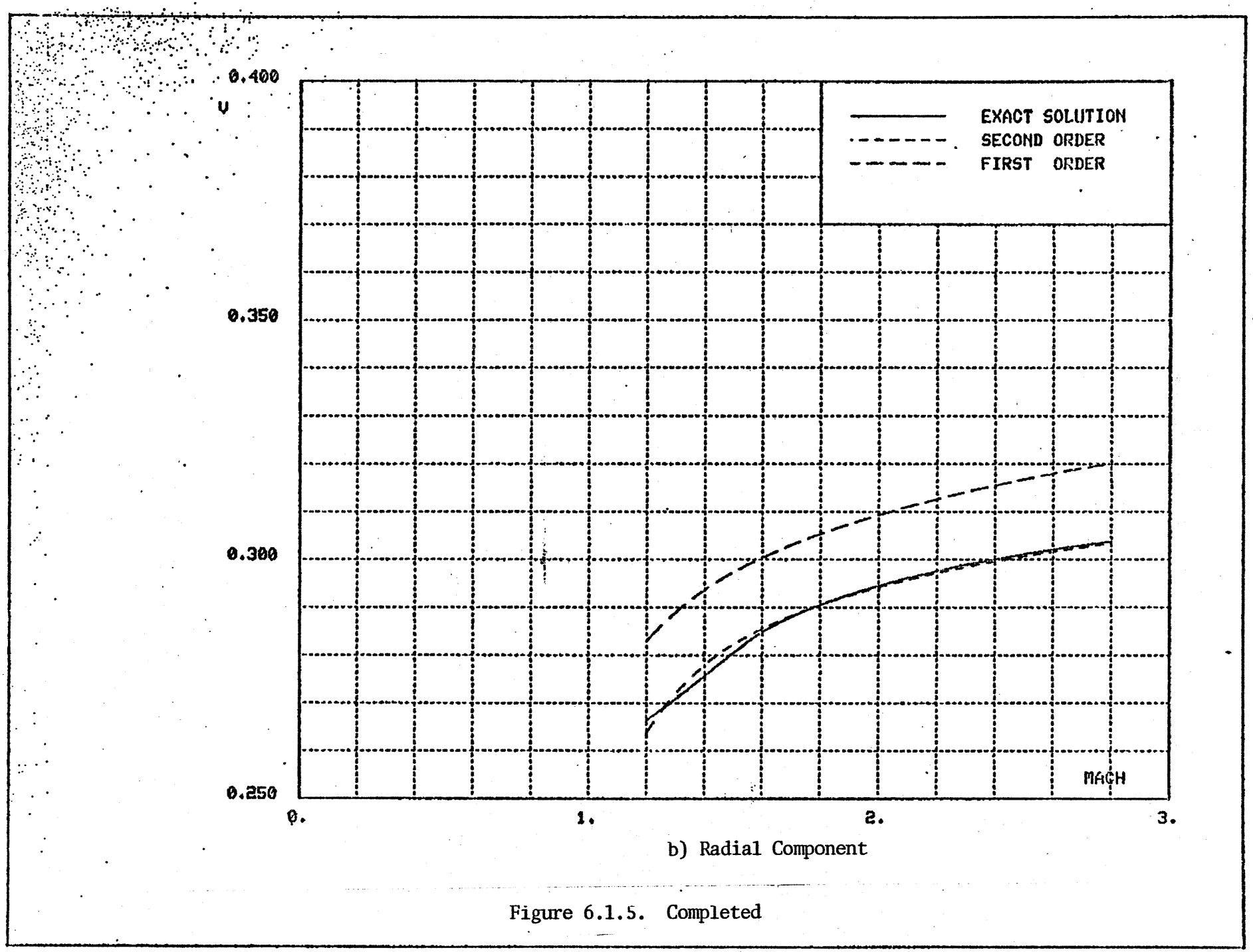

b) Radial Component

Figure 6.1.5. Completed

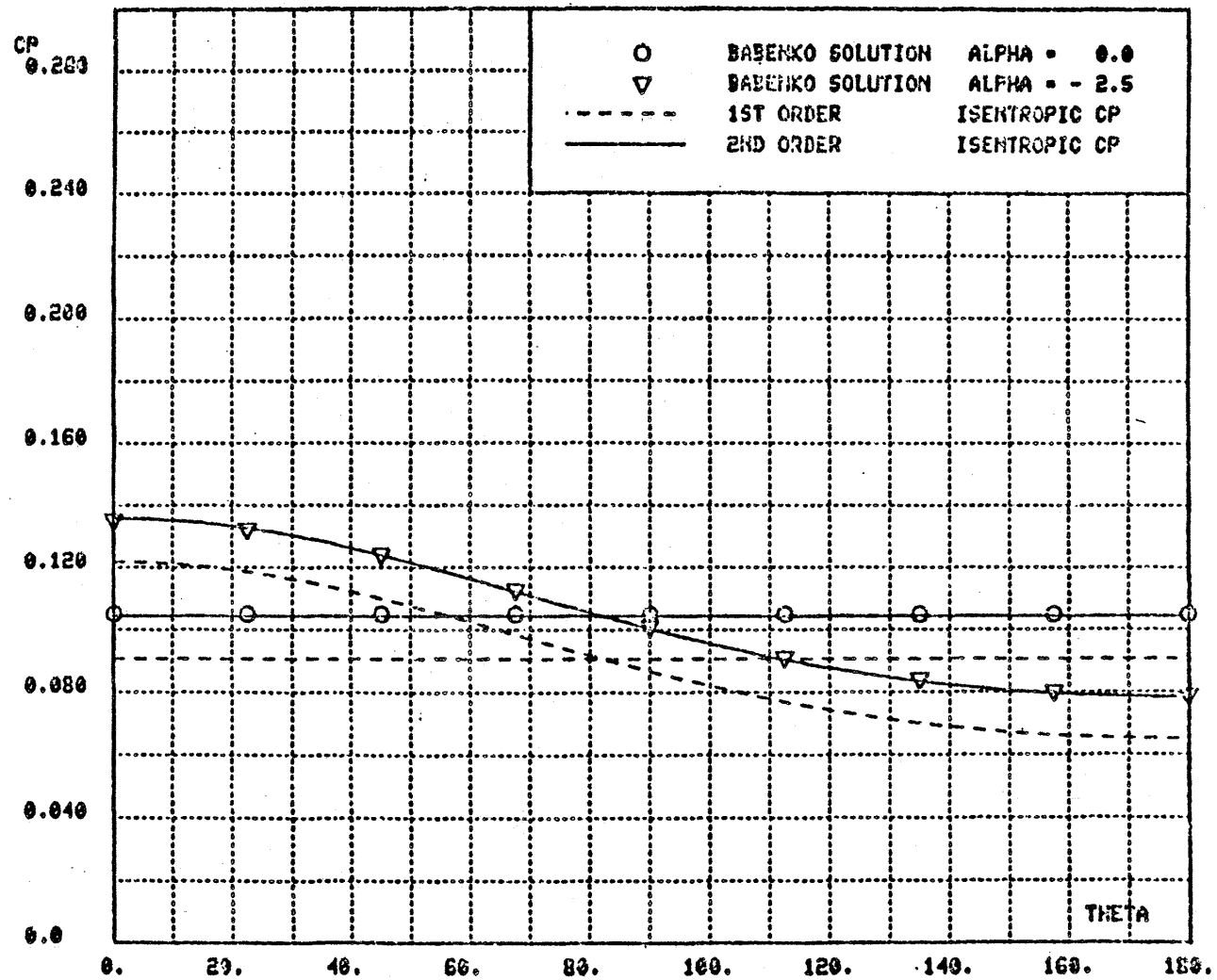

a) M = 2.0

Figure 6.1.6. Surface Pressure for a 10 Degree Cone

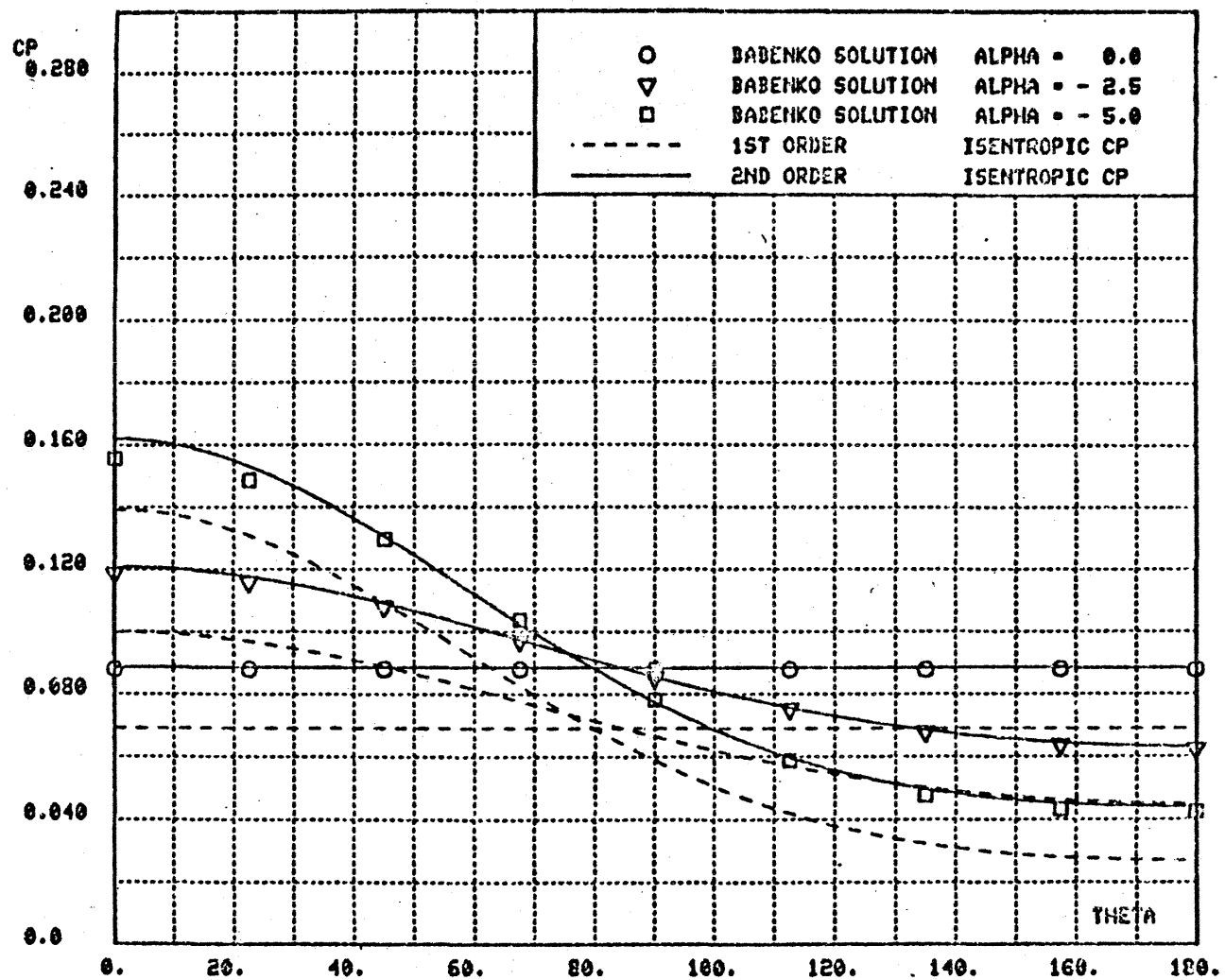

b) M = 3.0

Figure 6.1.6. Continued

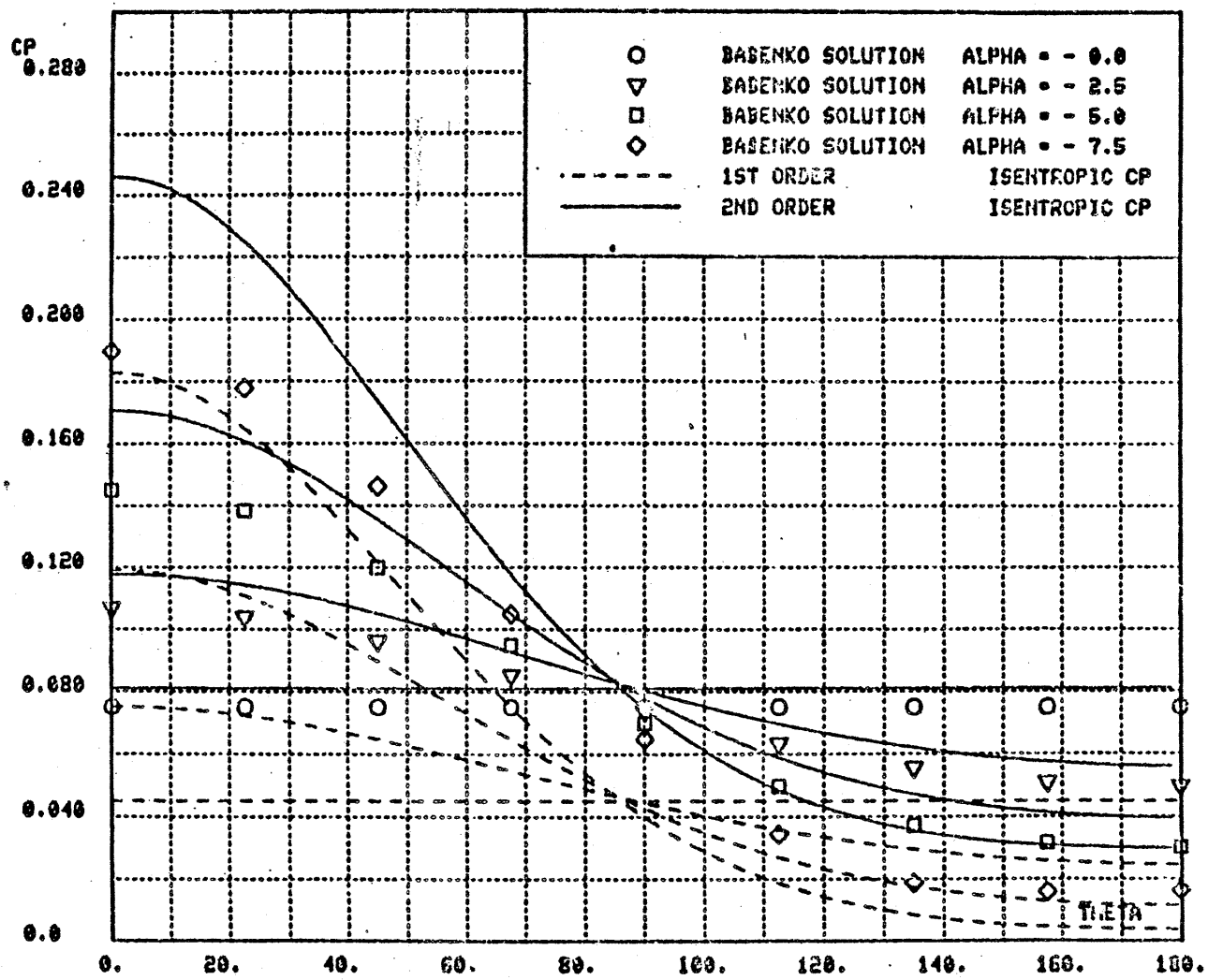

c) M = 5.0

Figure 6.1.6. Completed

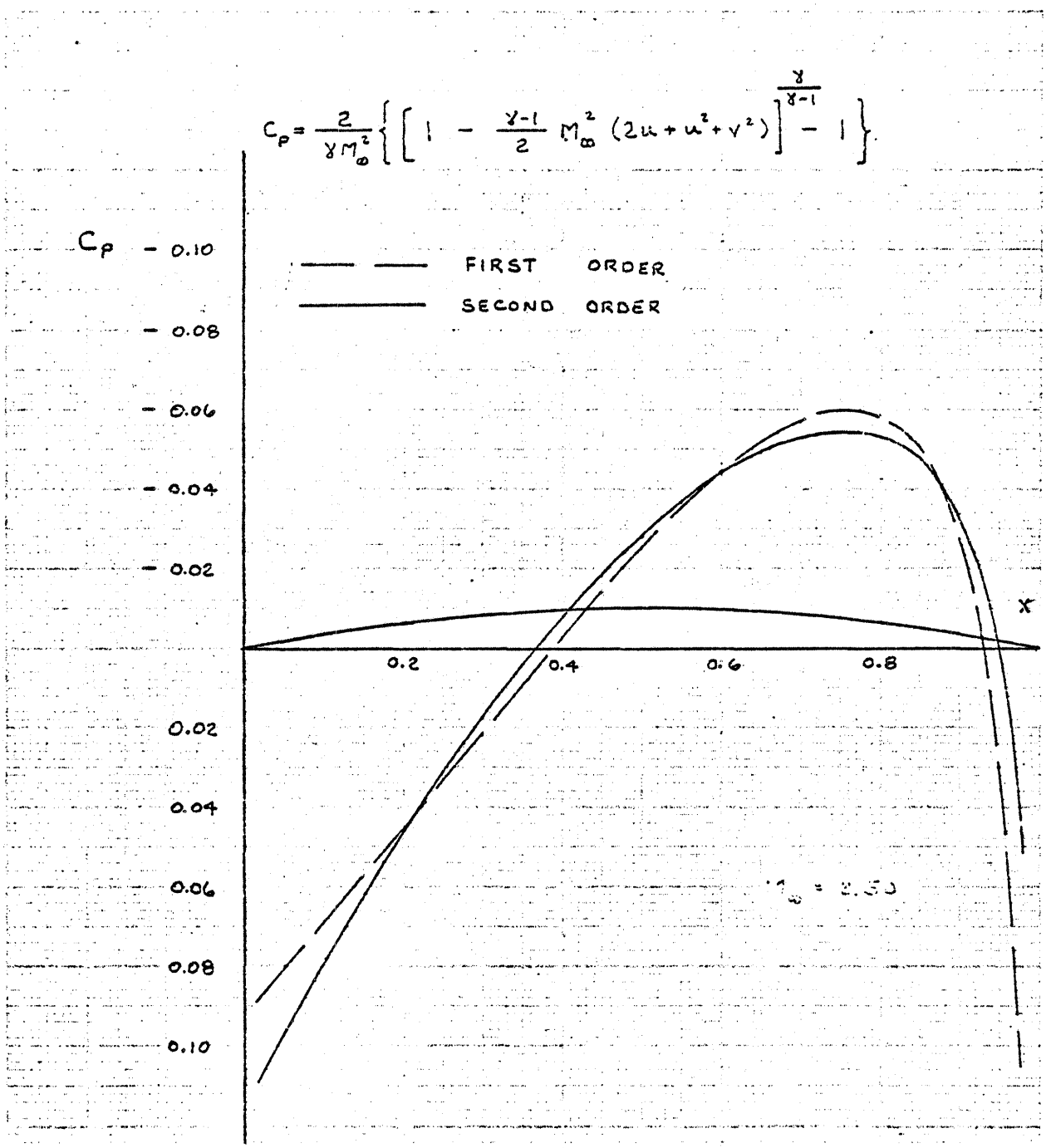

a) Mach 2.5

Figure 6.1.7. Comparison of First and Second Order Predictions for a Fineness Ratio 10 Parabolic Body of Revolution

$$C_p = \frac{2}{\gamma M_\infty^2}\left\{\left[1 - \frac{\gamma-1}{2} M_\infty^2 \left[2u + u^2 + v^2\right)\right]^{\frac{\gamma}{\gamma-1}} - 1\right\}$$

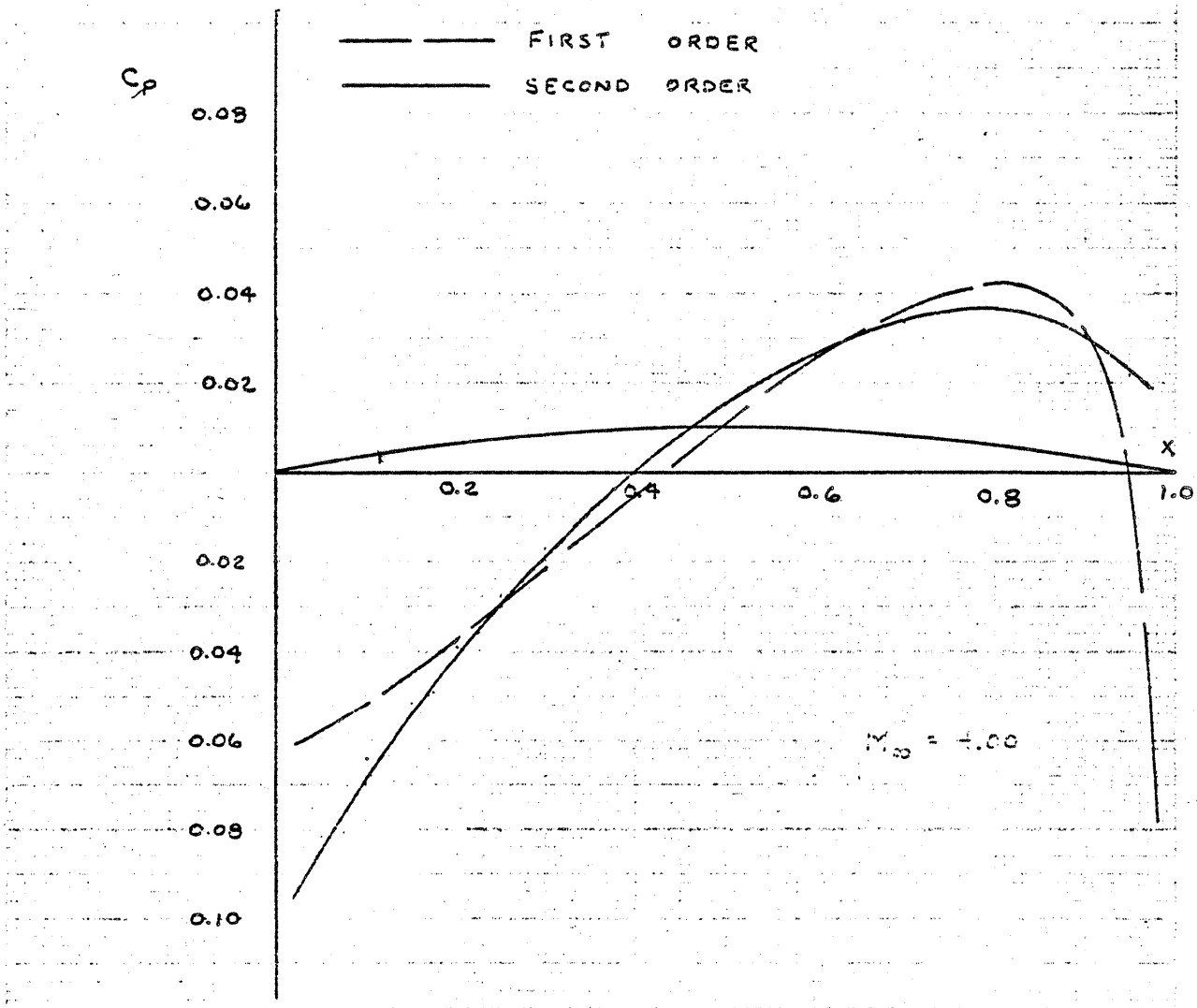

b) Mach 4.0

Figure 6.1.7. Completed

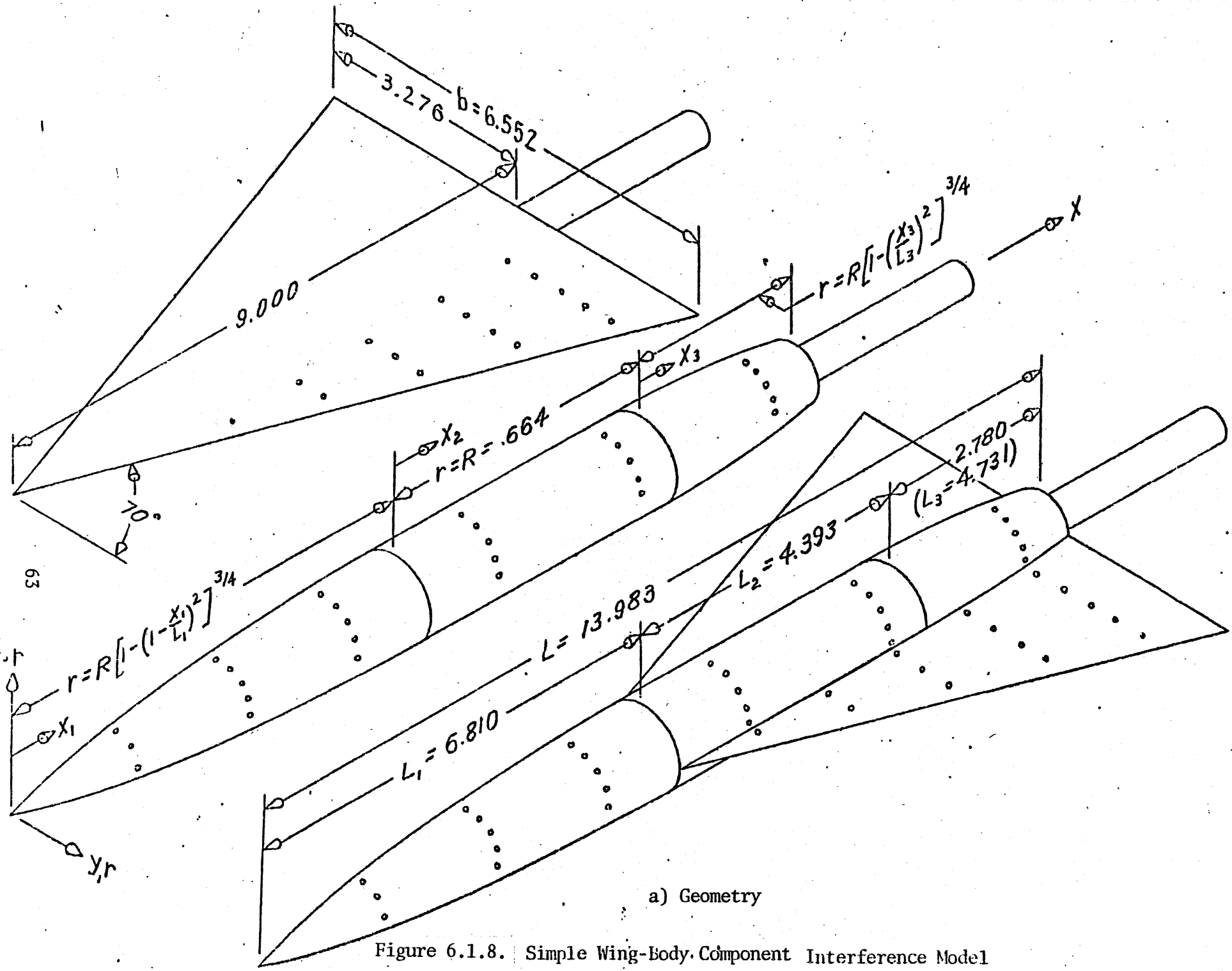

a) Geometry

Figure 6.1.8. Simple Wing-Body Component Interference Model

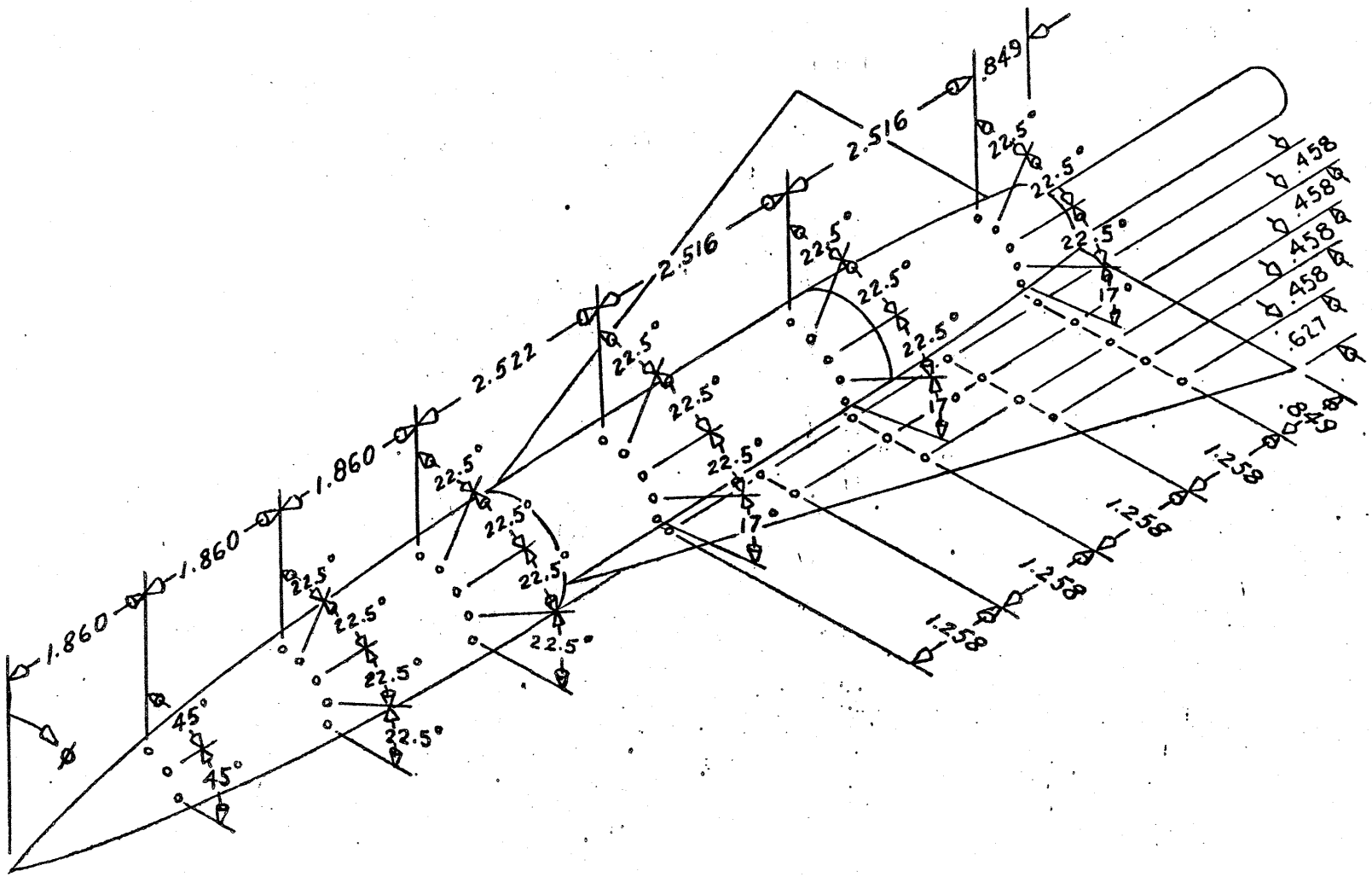

b) Pressure Tap Locations

Figure 6.1.8. Completed

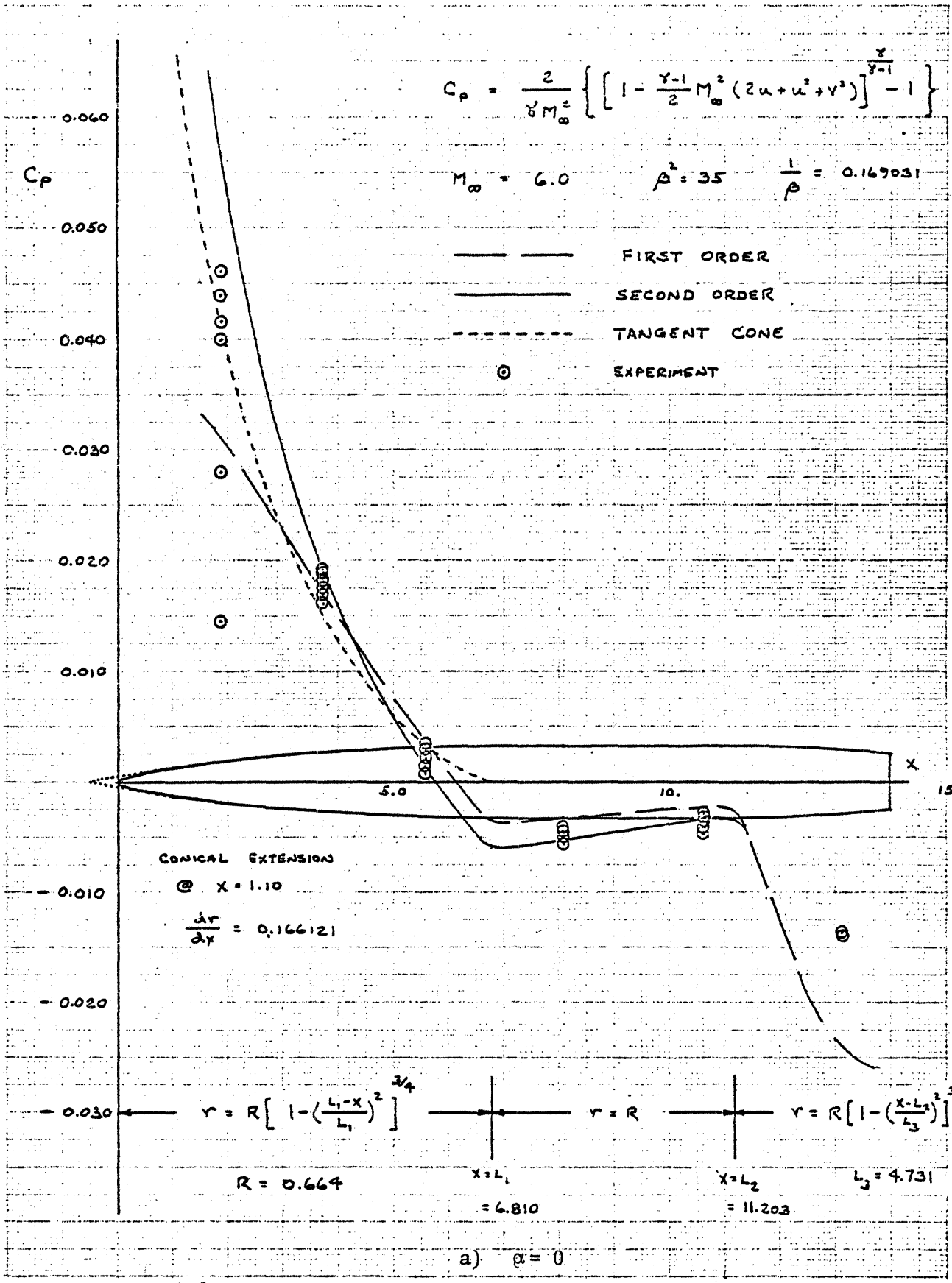

a) $\alpha = 0$

Figure 6.1.9. Comparison of Predicted and Measured Surface Pressures for a Body Alone at M = 6.0

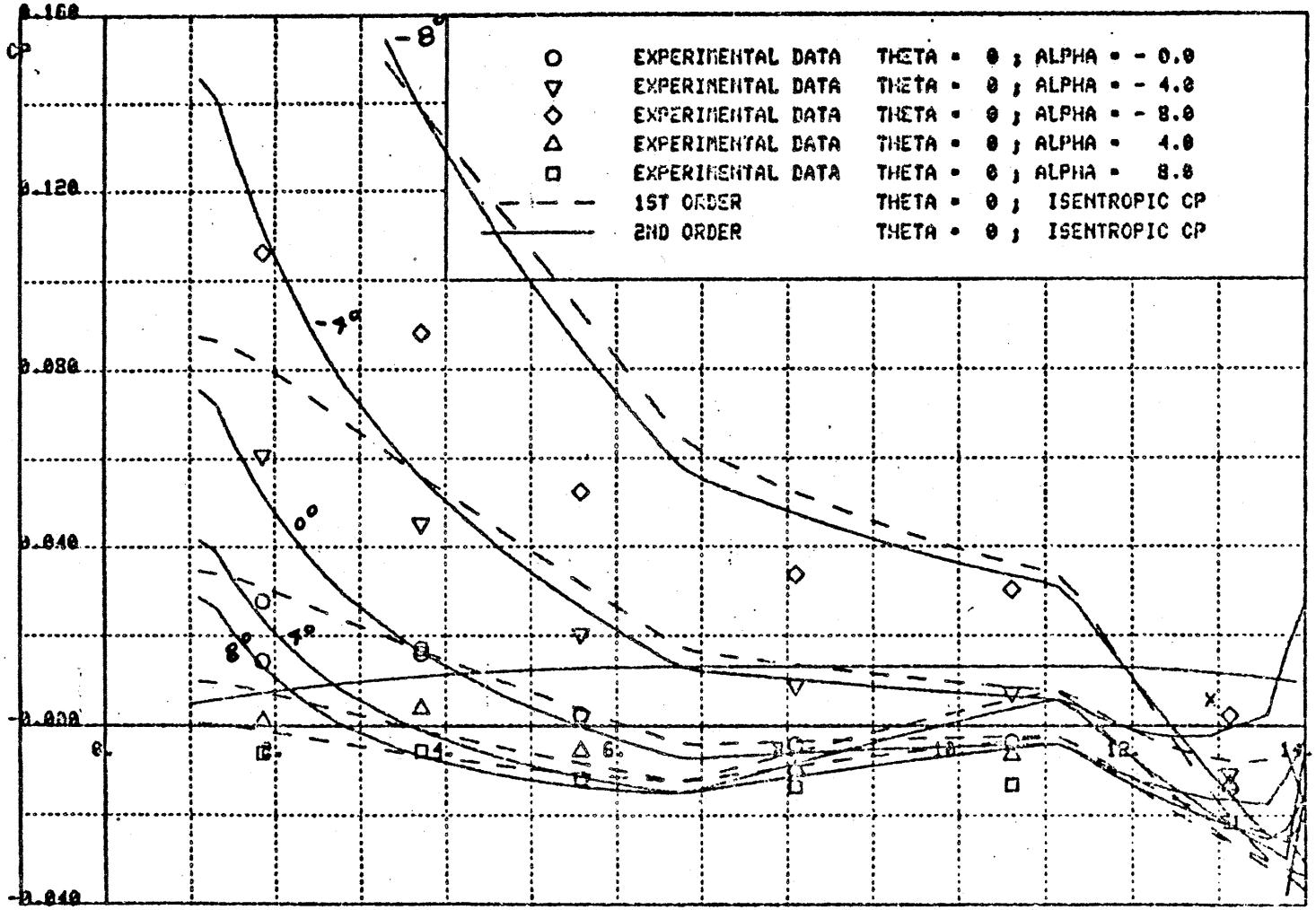

b) α variable, $\theta = 0$

Figure 6.1.9. Continued

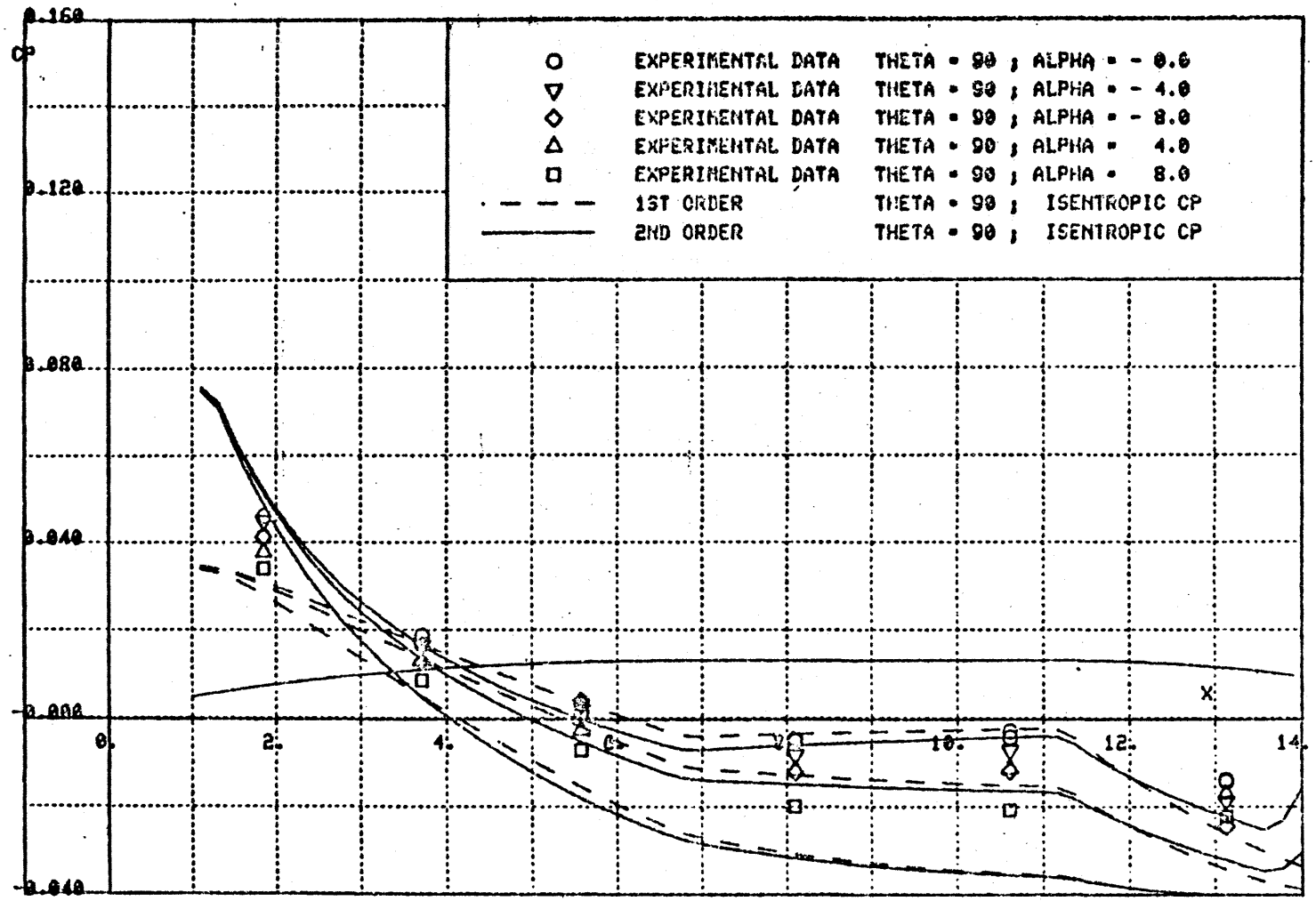

c) α variable, θ = 90°

Figure 6.1.9. Completed

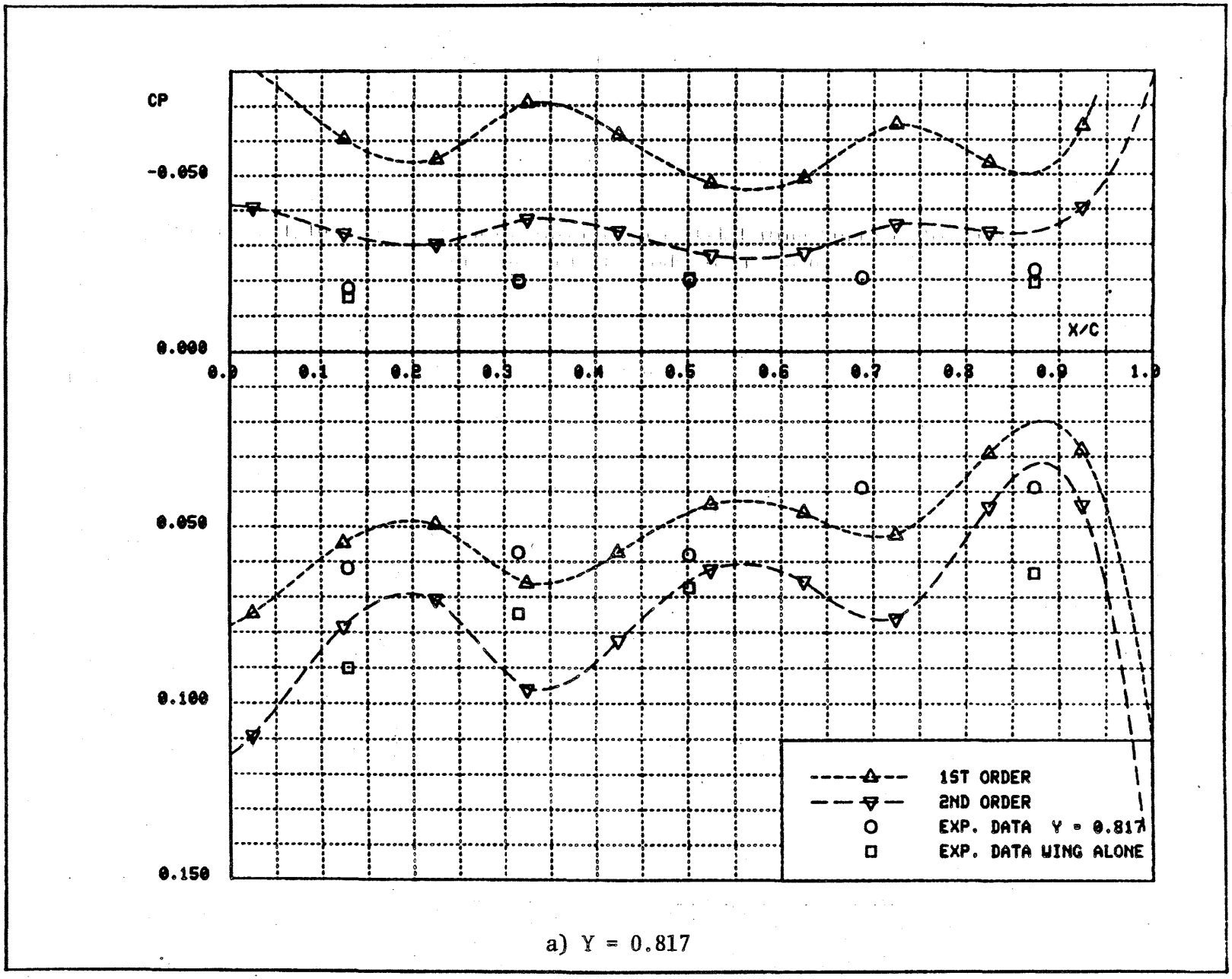

a) Y = 0.817

Figure 6.1.10. Comparison of Interference Model Wing Surface Pressures in the Presence of the Body at M = 6.0, α = 8°

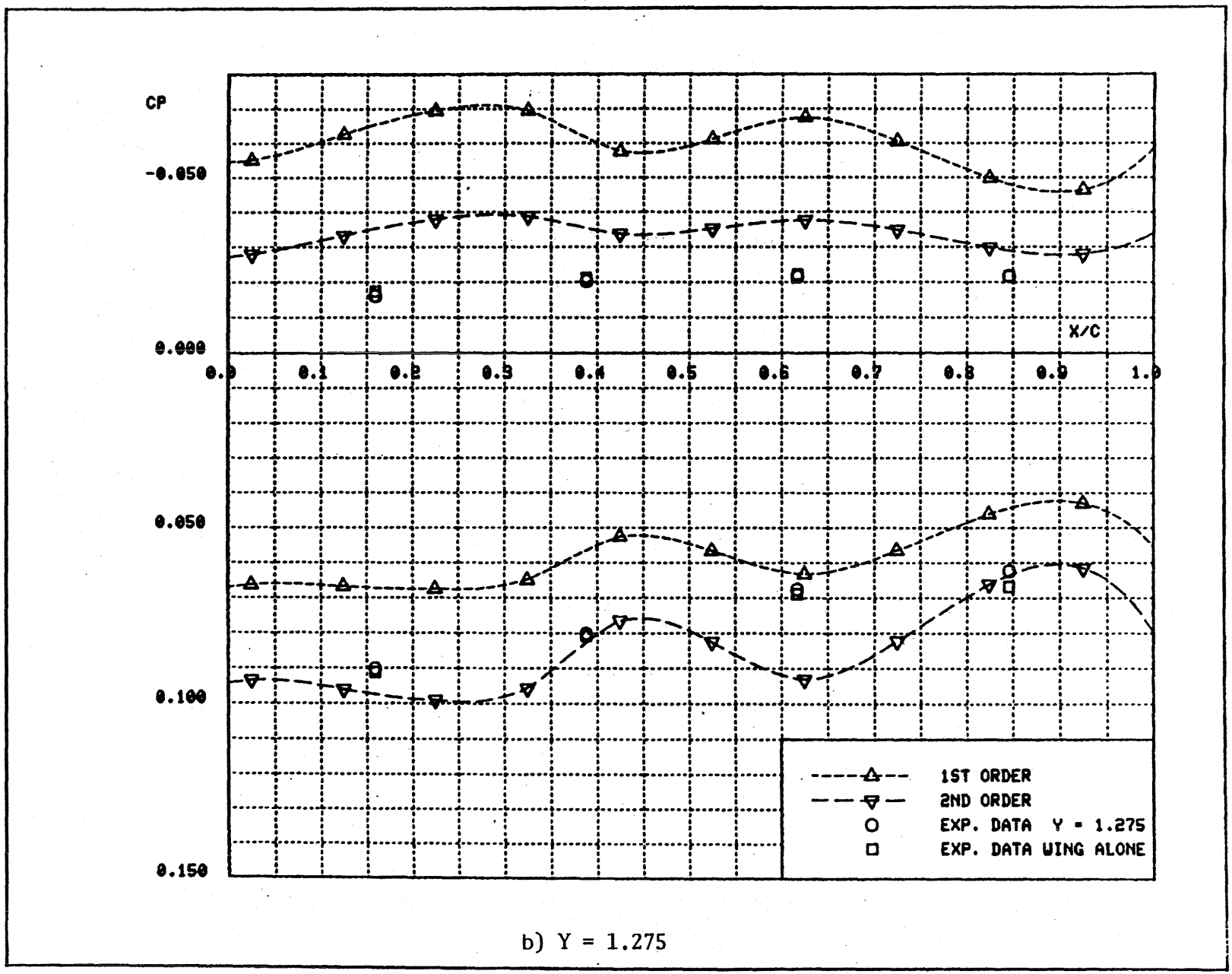

b) Y = 1.275

Figure 6.1.10. Continued

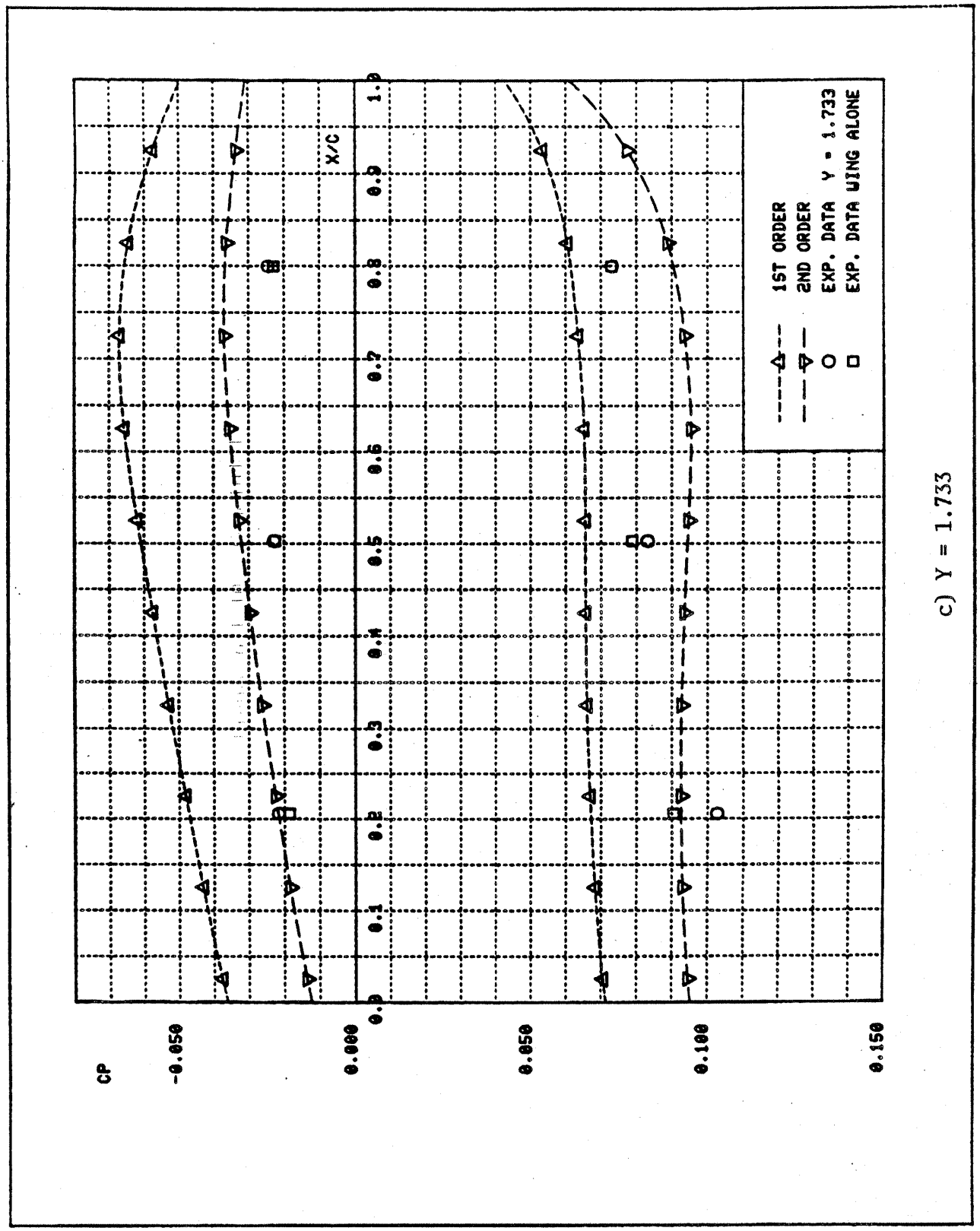

c) Y = 1.733

Figure 6.1.10. Concluded

6.2 FULL POTENTIAL COMPARISONS

In this section, results will be presented for both the full potential vector approach (Section 5.1) and the full potential scalar approach (Section 5.2). To verify the validity of the full potential theory, results are presented for various unit problems such as supersonic flow over two-dimensional wedge, supersonic leading edge delta wing, subsonic leading edge delta wing, and a simple conical wing-body combination.

6.2.1 Conical Wedge Flow

Figure 6.2.1 shows the schematic diagram of supersonic flow past a wedge with an attached shock wave. To implement the vector approach, a conical transformation of the independent variables was chosen to align the shock with a constant coordinate line.

$$\left.\begin{aligned} \sigma &= x \\ \xi &= y/x \end{aligned}\right\} \qquad (6.2.1)$$

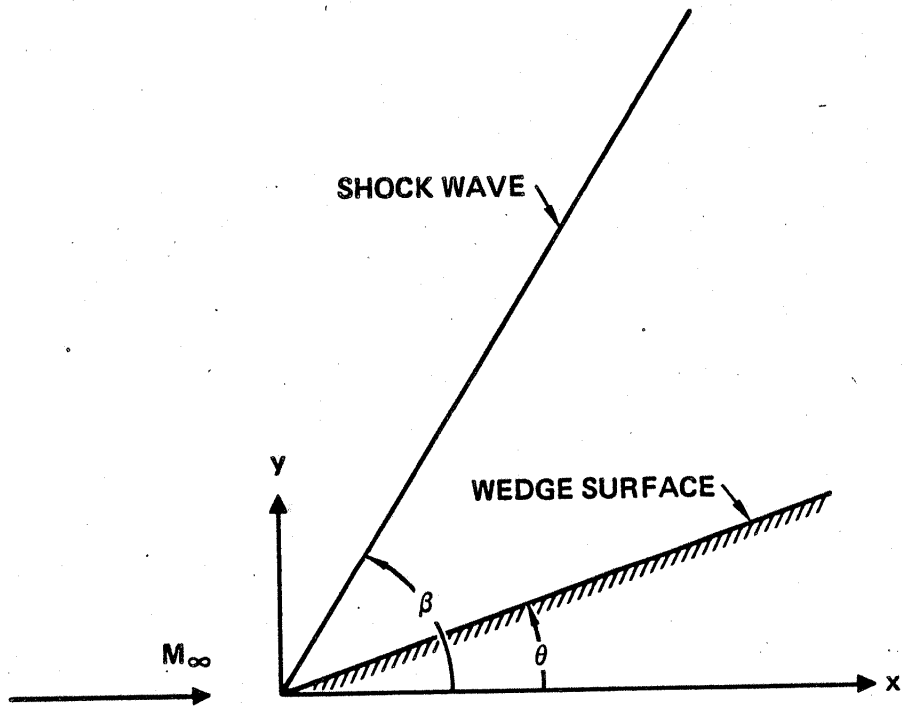

Figure 6.2.1. Schematic Diagram of Supersonic Flow Past a Wedge

This transformation coupled with the use of the strong conservation law form of the vector equation (5.11), and the conservative differencing provided by the MacCormack scheme, results in fairly weak oscillations across the shock.

To start the solution procedure, freestream values are specified at all grid points at an initial x location ($x = 1.0$). The solution is then marched along the x direction until an asymptotic steady state is reached. Care is taken to make sure that the grid points chosen enclose the shock. Freestream values are maintained at the outer boundary while surface tangency is imposed on the wedge boundary.

A comparison of the solutions obtained by using the Euler equation, the vector approach full potential equation (Eq. (5.11)), and the Cartesian scalar approach (Eq. (5.33)), is shown in Fig. 6.2.2. The results from the Euler and full potential vector approach show noticeable oscillations across the shock wave while the scalar approach seems to provide smooth monotone results. For this simple supersonic wedge flow example, the scalar approach demonstrated at least a factor of 10 speed-up in the computational time over the Euler solver as well as the vector approach. Also shown in Fig. 6.2.2 are the theoretical linear and second order solution.

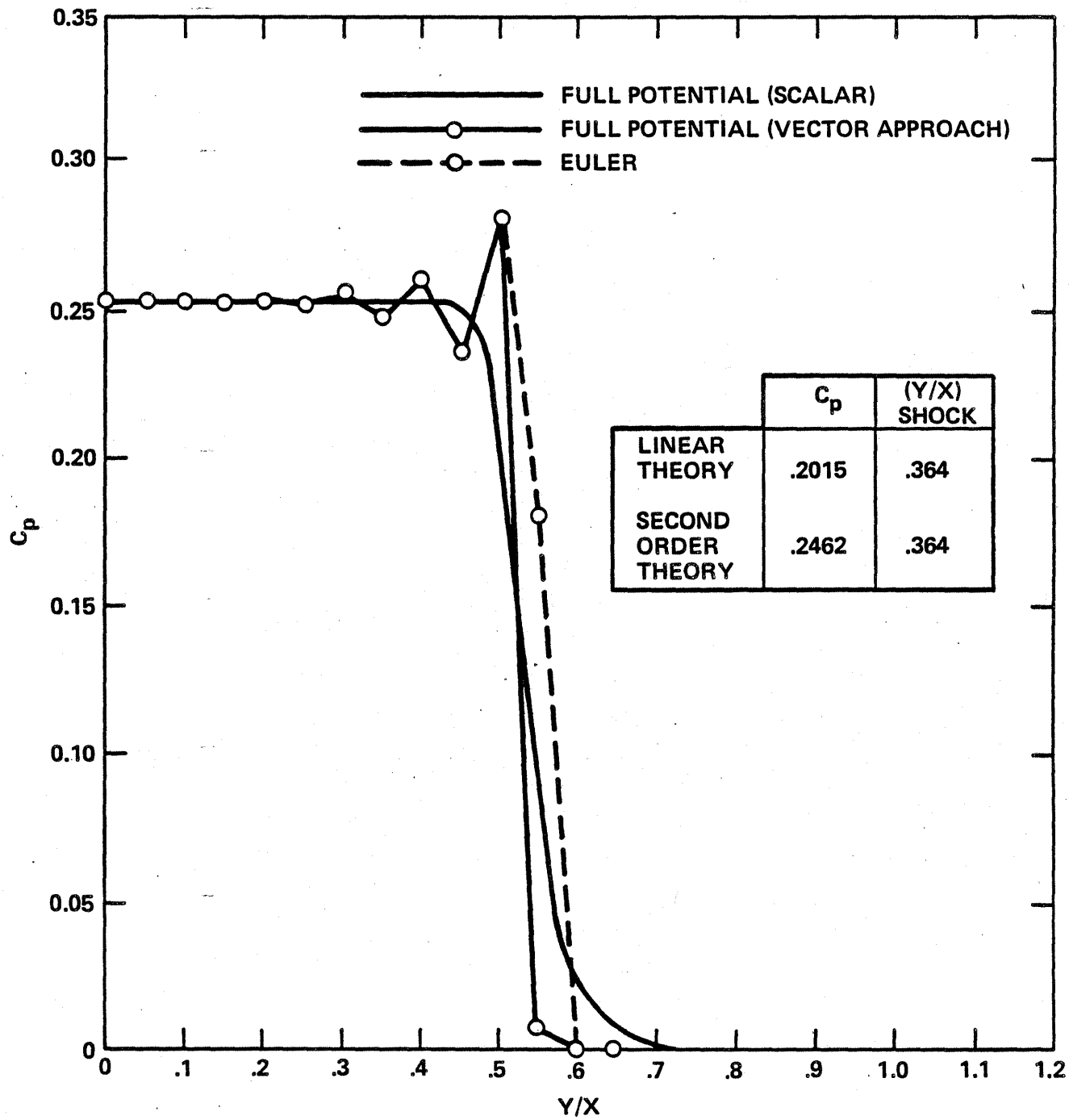

Figure 6.2.2. Supersonic Flow Past Wedge: Numerical Solutions

6.2.2 Supersonic Leading Edge Delta Wing

For a flat plate delta wing with a supersonic leading edge, the solution on the windward and leeward sides are independent of each other. We will study the windward or compression side in this report for this will test the numerical method's ability to capture three dimensional shocks and also check out the equations developed to fit the leading edge shock (see Fig. 6.2.3 for a schematic view of the flow field). For both shock capturing and shock fitting calculations, an initial solution is specified on an initial data plane at $x = 0.1$. The solution is then advanced downstream until it converges to a conically similar steady state.

6.2.2.1 Shock Capturing

The coordinate transformations used in the calculations where the shock is captured are

$$\sigma = x$$

$$\xi = z/x \qquad (6.2.2)$$

$$\eta = y/(x - z \tan \Lambda)$$

The constant coordinate lines in the physical and computational domains are sketched in Fig. 6.2.4. Freestream values are

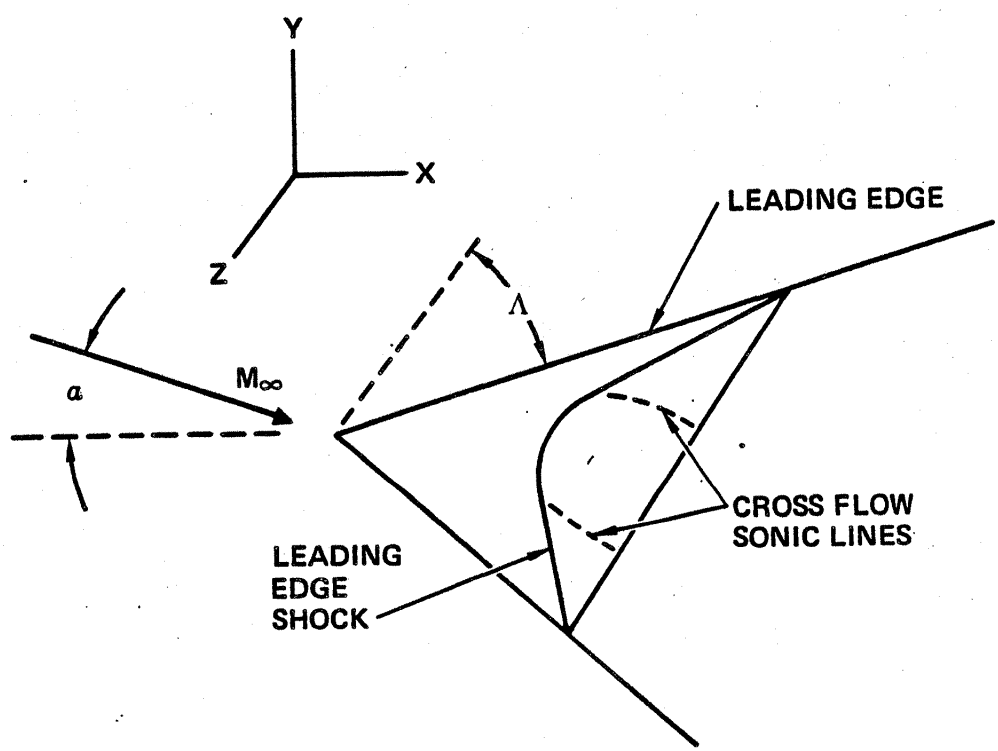

Figure 6.2.3. Schematic Diagram of Delta Wing Flow Field

specified at all grid points in the initial data plane. For this coordinate system it is advantageous to specify zero derivatives in the ξ direction at the boundary BC where the flow is two-dimensional.

6.2.2.2 Shock Fitting

The coordinate transformations used in the calculations where the shock is fit are given by

$$\sigma = x$$

$$\xi = z/x \tag{6.2.3}$$

$$\eta = \frac{y - y_{body}}{y_{shock} - y_{body}}$$

The corresponding constant coordinate lines are sketched in Fig. 6.2.5. The exact two-dimensional solution is imposed on the boundary BC at every marching step. The shock jump relations are imposed at the shock boundary CD. To start the calculations, an initial shock shape is chosen which determines the solution at all grid points on CD. At every spanwise grid point the initial values of the dependent variables are assumed to be those at the corresponding shock grid point. The shock slope at C is fixed at the exact value for all steps.

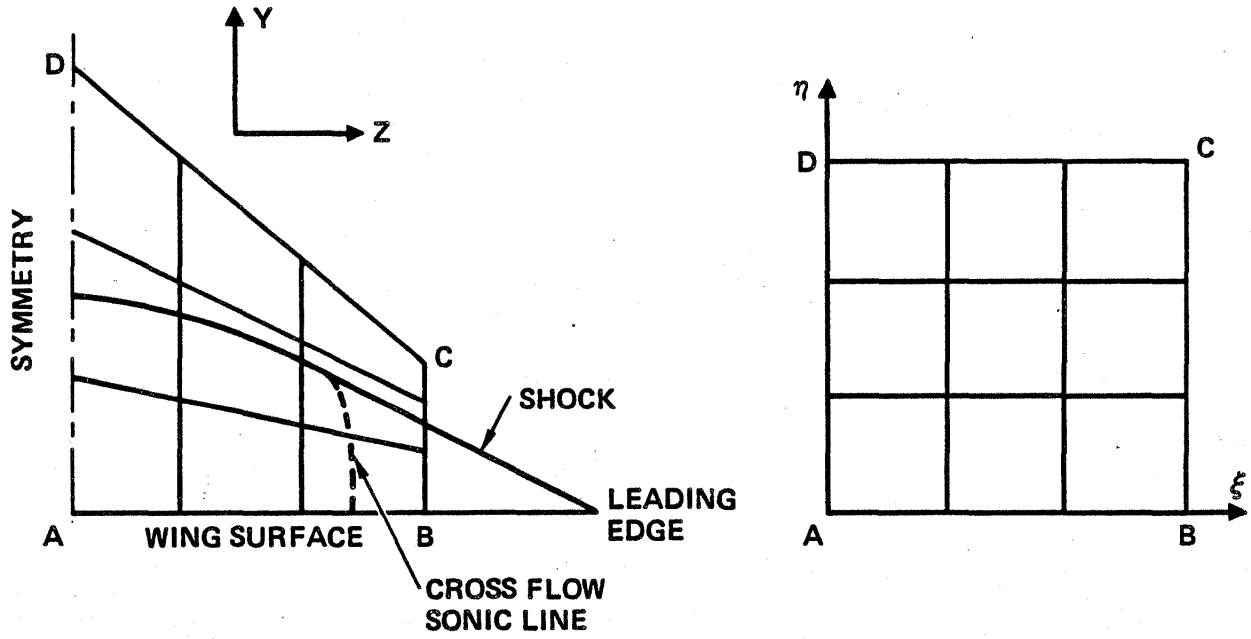

Figure 6.2.4. Computational Grid for Shock Capturing

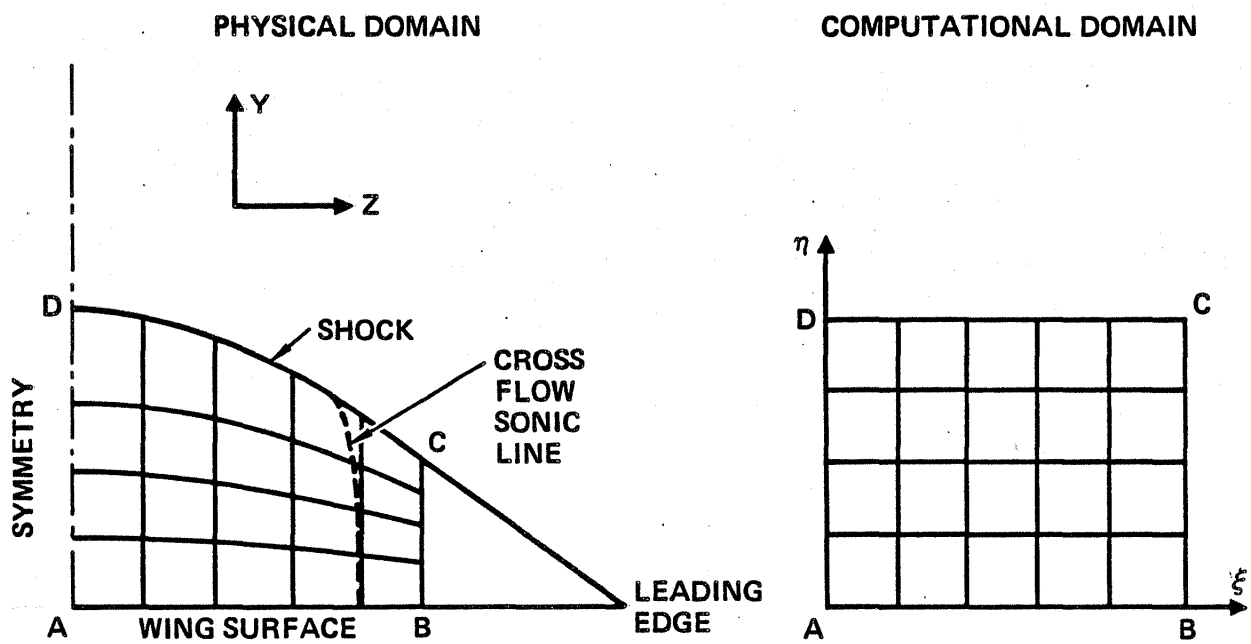

Figure 6.2.5. Computational Grid for Shock Fitting

For the vector approach, both the shock capturing and shock fitting schemes were implemented while the scalar approach results presented here are based on shock capturing procedure. In Fig. 6.2.6, pressure coefficient results from the full potential vector and scalar approach are compared with results obtained with a shock capturing Euler solver and second order potential theory for $M_\infty = 4.0$, $\Lambda = 50°$ and $\alpha = -5°$, $-10°$ and $-15°$. Although the full potential scalar approach and vector approach predict identical results, the scalar approach is an order of magnitude faster than the Euler or the full potential vector approach. For low angles of attack ($\alpha = -5°$), the full potential solution is indistinguishable from the Euler solution.

From comparing the second order theory solution with the FPE and the Euler solutions, the inability of the second order theory implementation to shift the cross flow sonic line (junction of the two-dimensional and three-dimensional regions) becomes clear. The FPE is superior in this respect, as far as producing results comparable to Euler solvers.

6.2.3 Subsonic Leading Edge Delta Wing

One of the advantages of full potential theory over the linear or second order theory is that it does not create any leading edge singularities, and thus can easily

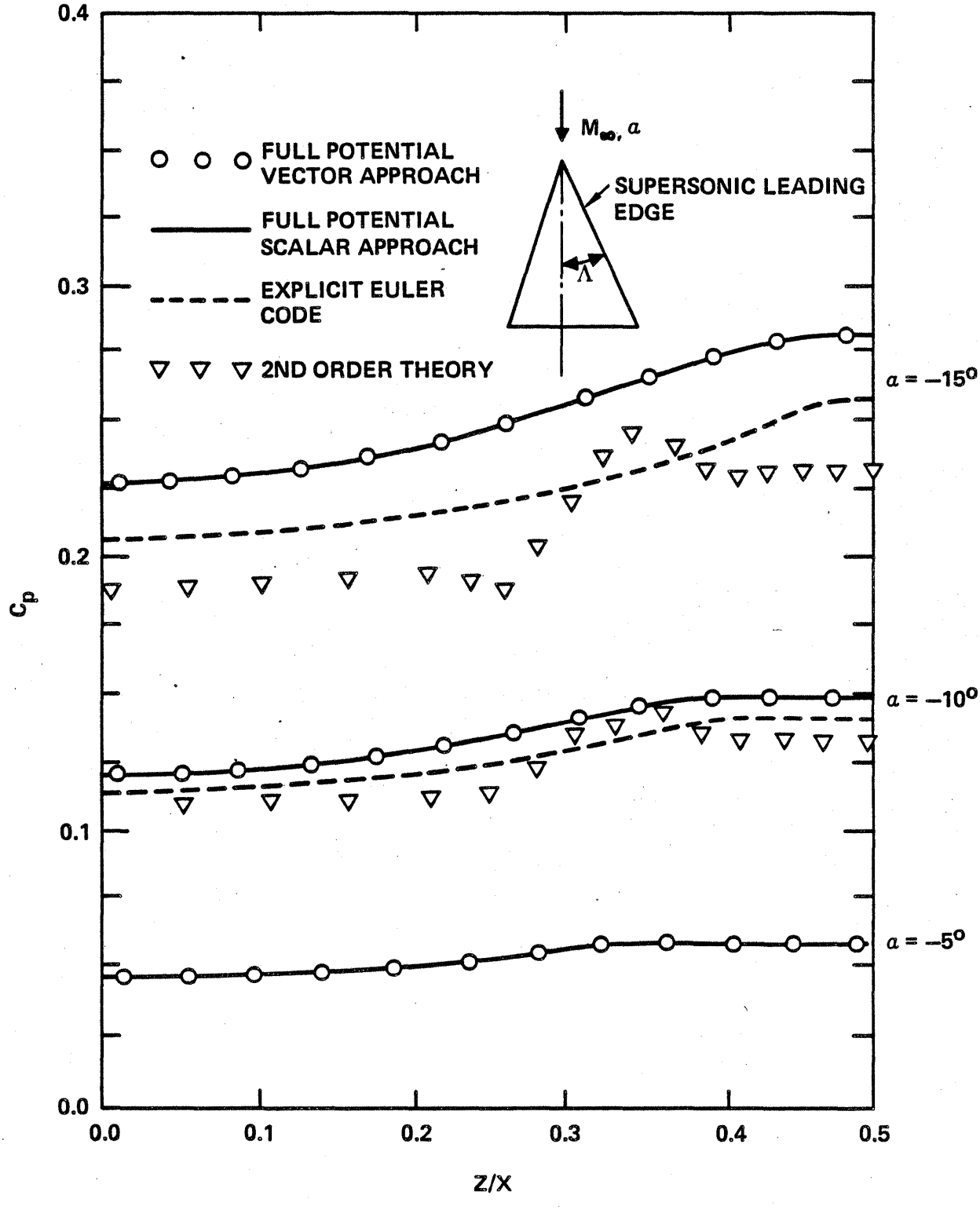

Figure 6.2.6. Comparison of Pressure Coefficient on Supersonic Delta Wing at Various Angles of Attack, $M_\infty = 4.0$, $\Lambda = 40°$

handle subsonic leading edges. The second order finite difference results for the subsonic leading edge cases are shown in Ref. 1 which indicate pronounced oscillations in pressure in the neighborhood of the leading edge because of the singularity inherent in the theory. This behaviour is avoided by using full potential theory as illustrated in Figs. 6.2.7 and 6.2.8. Figure 6.2.7 shows the results obtained using the full potential vector approach. All four cases (λ = 20°4', 28°50', 38°39' and 43°38') are presented. There are no oscillations in the surface pressure coefficient. Some breaks in smoothness are evident near the leading edge on the wing surface. Tests reveal that this is due to the discontinuity in the grid used (analytic metrics were also used for these calculations and so the mesh was not implicitly smoothed out by the numerical evaluation of metrics). For the low freestream Mach number of 2 considered, tests showed that the solutions to the FPE and Euler equations are indistinguishable because of the negligible entropy generation. However, this would be true even for higher Mach numbers for slender delta wings with subsonic leading edge because the leading edge compression system is relatively weak for these cases except possibly when the leading edge is very close to the Mach cone associated with the freestream Mach number.

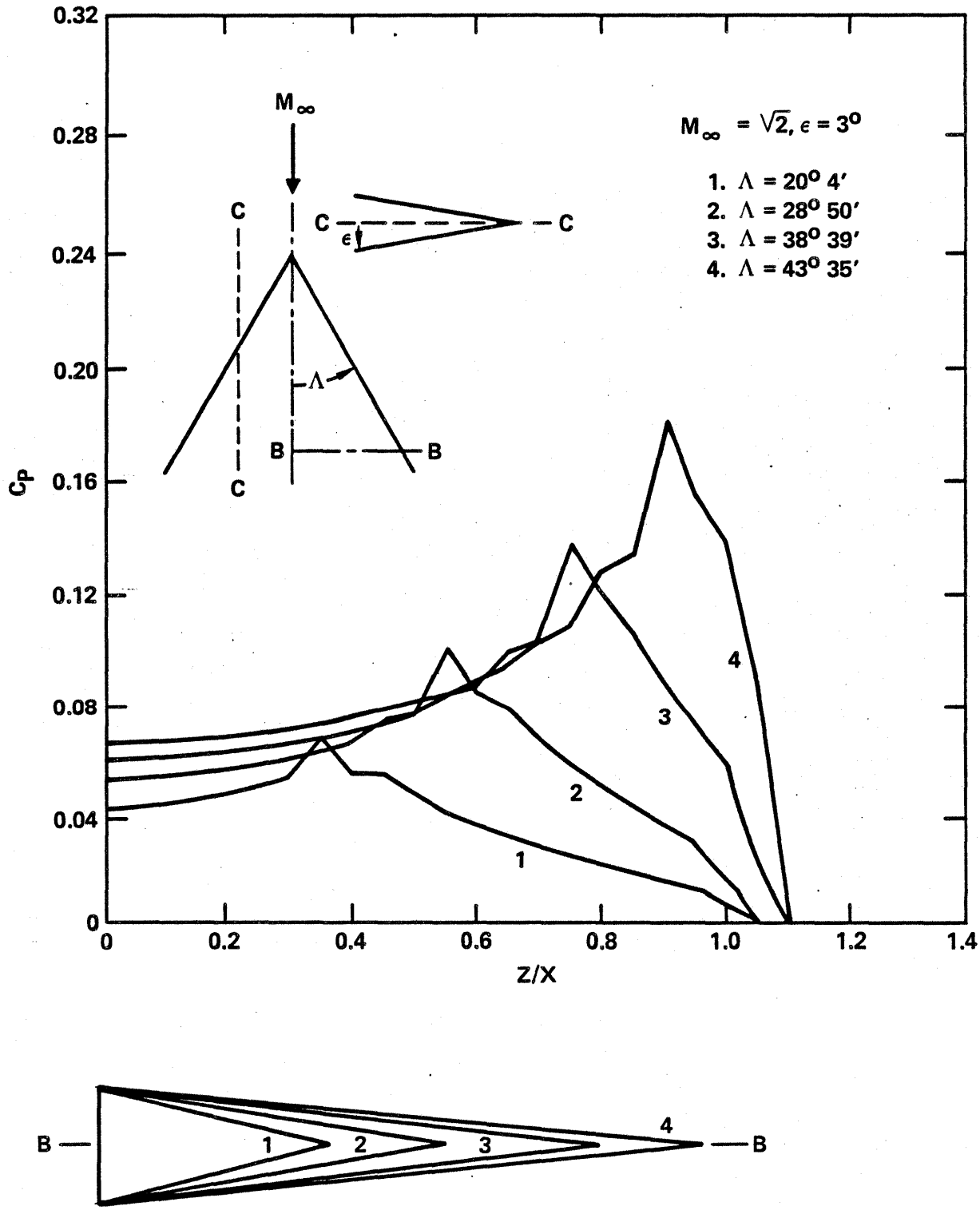

Figure 6.2.7. Pressure Coefficient on Series of Delta Wings with Subsonic Leading Edges using the Full Potential Vector Approach

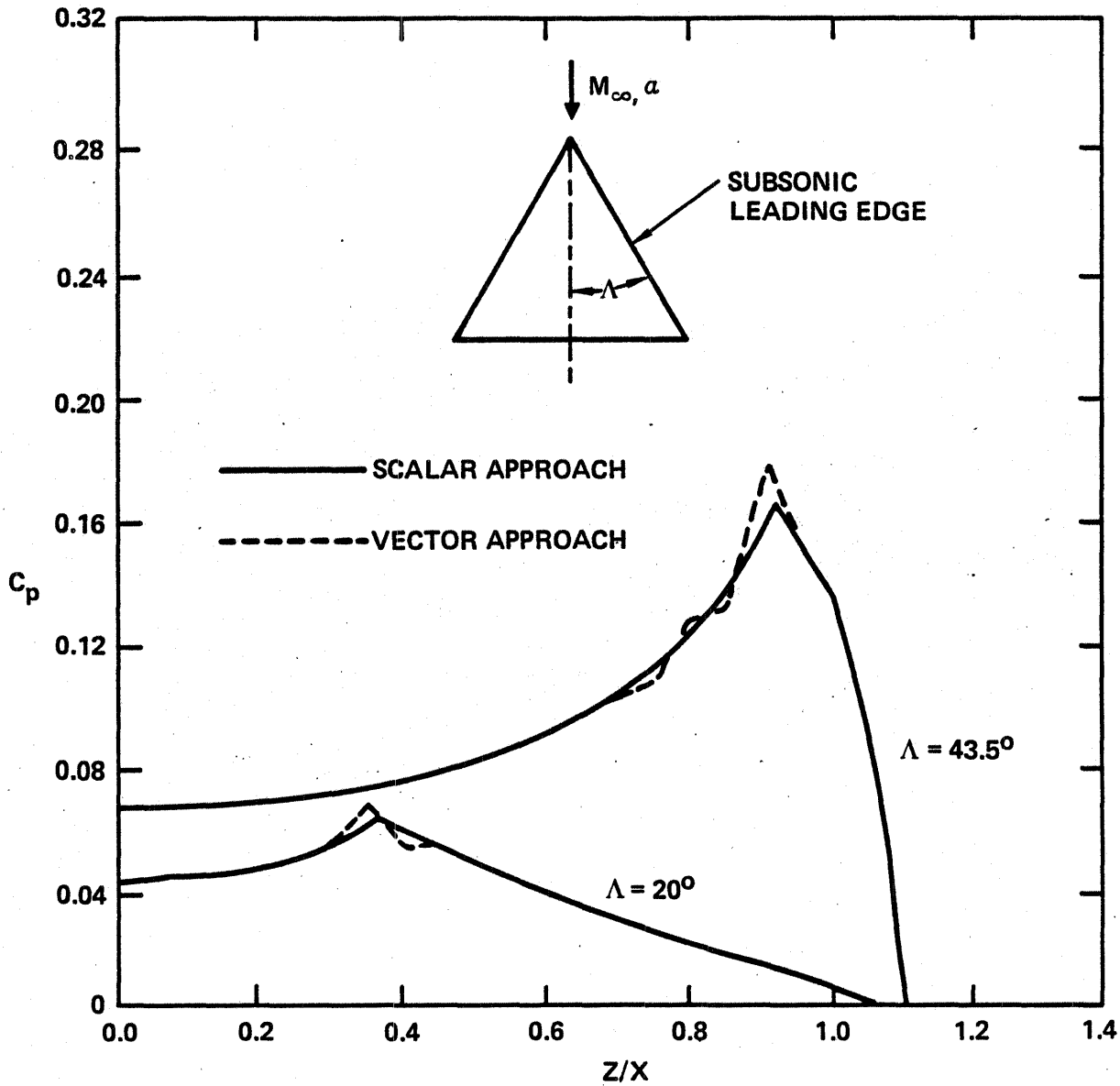

Figure 6.2.8. Pressure Coefficient on Delta Wings with Subsonic Leading Edge using the Full Potential Equation, $M_\infty = 2$, $\alpha = 3°$

The results from the full potential scalar approach are compared in Fig. 6.2.8 with the vector approach results. The scalar approach results are much superior and also required much less time to compute over the vector approach.

6.2.4 Cosine Wing-Body Combination

The wing-body configuration consisted of a flat plate delta wing with a conical fuselage represented by the formula

$$\frac{y_{body}}{x} = \frac{0.1678}{2}\left(1 + \cos\frac{\pi z}{0.2098x}\right) \quad 0 \leq \frac{z}{x} \leq 0.2098 \ .$$

The shock capturing versions of the finite difference methods using the Euler equation and the full potential vector and scalar approaches were used to compute the pressure coefficient on the surface of the wing-body combination and the results are shown in Fig. 6.2.9. It is evident that for the low angle of incidence considered here the full potential and Euler solutions are in good agreement. The scalar approach program utilizes a linearization of the actual body boundary conditions because the code at present is in terms of a Cartesian system in which the body is not in general aligned with grid points.

The results are in qualitative agreement with the results obtained by Kutler[5] for a similar geometry. The salient

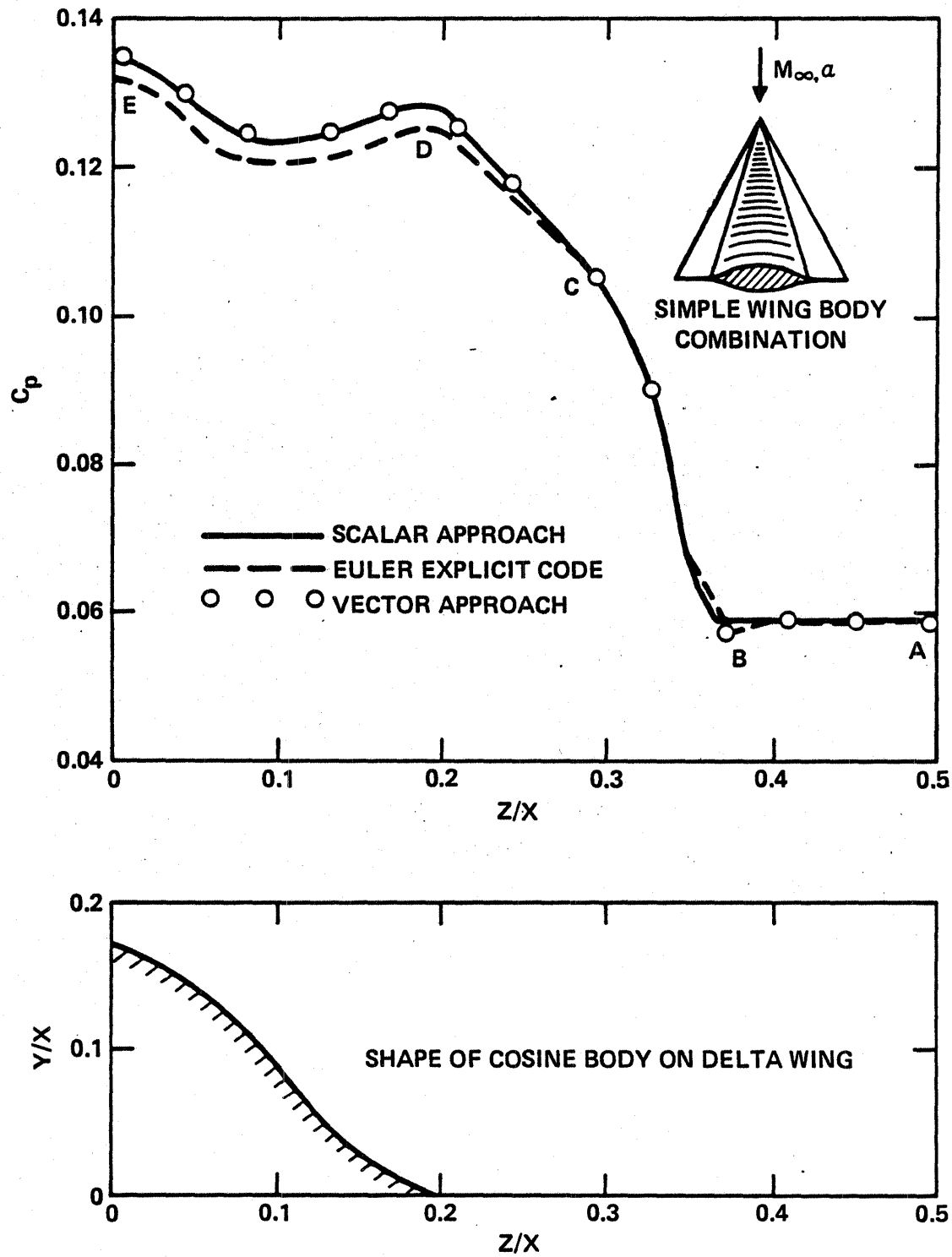

Figure 6.2.9. Hypersonic Flow past a Conical Wing-Body Combination, $M_\infty = 4$, $\alpha = 5°$, Compression Side.

features of the pressure distribution on wing-body combinations similar to the ones considered here are as follows: (1) A two-dimensional region between the supersonic leading edge and cross-flow shock (a part of which is shown as AB in Fig. 6.2.5). (2) A pressure rise across the cross-flow shock denoted by BC. (3) Compression up to the junction of wing and body denoted by CD. (4) An expansion followed by compression on the fuselage denoted by DE.

Here again the scalar approach demonstrated a significant (at least a factor of 10) improvement in computational speed over the Euler solver or the full potential vector approach.

7. CONCLUSIONS

Based on the theoretical development and comparison with higher order results/experimental measurements, the following conclusions are made.

1. Improved prediction of supersonic/hypersonic aerodynamic characteristics and surface pressures for a simple wing, body and wing-body shapes has been demonstrated for non-linear potential analysis.

2. Second order theory provides a systematic means of extending linear analysis to values of the similarity parameter $M\delta$ approaching one. Fifty second CPU solution time/Mach number is typical for a wing-body problem.

3. Full potential analysis successfully eliminates subsonic edge singularities and linear characteristic approximations of second order theory. The scalar formulation is an order of magnitude faster than the vector approach and Euler solvers.

4. Potential theory provides an advanced aerodynamic prediction technique that is responsive to the preliminary design problem at moderate hypersonic conditions.

5. Further effort is required to extend the analyses to more general geometries and develop configuration design codes.

8. REFERENCES

1. "Formulation of Aerodynamic Prediction Techniques for Hypersonic Configuration Design," NASA CR-158994, February 1979.

2. Van Dyke, M. D., "A Study of Second-Order Supersonic Flow Theory," NACA TN 2200, January 1951.

3. Gunness, R. C., Jr., Knight, C. J., and Sylva, E. D., "Flow Field Analysis of Aircraft Configurations Using a Numerical Solution to the Three-Dimensional Unified Supersonic/Hypersonic Small Disturbance Equations," NASA CR 1926, February 1972.

4. MacCormack, R. W., "The Effect of Viscosity in Hypervelocity Impact Cratering," AIAA Paper No. 69-354, Cincinnati, Ohio, 1969.

5. Kutler, P., "Computation of Three-Dimensional, Inviscid Supersonic Flows," in Lecture Notes in Physics 41, Springer-Verlag, New York, 1975.

End of Document